Master's Thesis of Engineering

Post-calibration of DTS data and analysis of well completion process monitoring in CO_2 geological storage demonstration site

DTS 자료의 후교정과 CO_2 지중저장 관측공 완결과정 모니터링 자료의 분석

August 2018

Graduate School of Engineering
Seoul National University
Department of Energy Systems Engineering

DASOM SHARON LEE

Abstract

Post-calibration of DTS data and analysis of well completion process monitoring in CO_2 geological storage demonstration site

Dasom Sharon Lee
Department of Energy Systems Engineering
The Graduate School
Seoul National University

The DTS temperature profiles obtained during well completion of Korea's first CO_2 monitoring well in Janggi, Pohang were analyzed to characterize each well completion process in terms of temperature anomalies and to evaluate the feasibility of DTS as a monitoring tool of well development process. Since DTS temperature, a measure of temperature effect on a scattering of light traveling in fiber, should be calibrated to real temperature and unavoidable depth mismatch during installation should also be corrected, several post calibration methods of depth and temperature are also investigated.

The unavoidable depth mismatch is corrected by applying conventional approach which subtracts the ratio of cable length error to TD (Total Depth) of well from each measurement depth, and confirmed its effectiveness by comparing the result

with the location of transition point of steel and FRP (Fiber-Reinforce Plastic) and its effect on temperature change pattern during gas lift.

For temperature correction, several point-wise methods and conventional long-point pre-calibration method are investigated to suggest an effective post-calibration method. The conventional method by submerging a portion of cable longer than the length of resolution cell defined by pulse width or a gauge length of a measurement system in water showed preferable result than the other methods. However, point-wise methods which gave reasonable and comparable results with long-point method also showed that it could be a useful alternative when a long-point method-based pre- & post-calibration cannot be done.

The real-time DTS monitoring data revealed that each well completion processes can be characterized by their own distinctive temperature anomaly patterns. In gravel packing, the progression up the well of the emplaced sand was noticeable as an anomaly and creating a thermal bridge to the warmer formation. The DTS data clearly shows the exothermic reaction associated with curing of cement within the cementing boundary. During gas lift operations, the conventional highly oscillating pattern was observed in the DTS data, but in our case, the casing transition point was delineated. In summary, these imply that real-time DTS monitoring could not only be an effective tool of monitoring but also controlling, and optimization of well completion procedure.

Keywords: distributed temperature sensing, DTS, distributed sensing, temperature calibration, depth calibration, fiber optic sensing, well completion, Janggi field

Student number: 2016-21301

Contents

List of Tables

List of Figures

Chapter 1. Introduction

1.1 Background

The temperature logs have been used to monitor events inside the wells since 1930 to understand the events inside the well by measuring the fluid temperature, mainly for monitoring and production logging. However, the point sensor was limited to obtaining sections of the well as it can only measure the temperature around the sensing component and only available during production logging (Schlumberger, 2009). The point sensor limited our understanding of the events happening inside well as it can only monitor an anomaly after an event and cannot measure temperature as the event is occurring. Obtaining temperature through logging was time-consuming because the temperature sensor had to be continuously lowered as a moving probe at known depth to obtain temperature values (Hurtig, 1995). It also suffered from electric magnetic noise for long distance measurement. Therefore, point temperature sensing was restricted to understanding the events inside the well and therefore not suitable for continuous temperature profile measurement (Wang, 2013).

The first temperature distributed sensor was demonstrated by Hartog (1982) using liquid-core fiber but had limited practical application in deployment and restricted temperature range. The distributed sensing has evolved as a practical application using inelastic scattering for temperature, strain, and vibration measurement. The fiber optic distributed temperature sensing (DTS) technology overcame the limitation of the point sensing technology by allowing spatial continuity of the temperature profile as the fiber itself is the sensing medium. It enabled continuous

real-time temperature profile at any time throughout the well, once it is permanently installed inside the well (Hurtig, 1995). Unlike the production logging run, which obtains temperature after the event, the DTS can identify changes in-well performance as the event occurs during production and shut-in (Schlumberger, 2009). Therefore, the DTS data can display changes inside the well with reservoir condition changing. The fiber optic distributed sensing has many more advantages compared to conventional point sensor as it can be deployed in any harsh or unusual environments because of its small, light, corrosion–resistance, long sensing range, good sensitivity, and immune to electromagnetic interference.

1.2 Research Objectives

The distributed temperature sensing is a powerful tool in obtaining continuous heat profile of the well and valuable tool in understanding the events inside the well. However, it only measures relative temperature and requires calibration to the true temperature. The DTS data obtained from Janggi field site in Pohang faced difficulty interpreting the rapidly changing temperature and variations inside the well during completion due to calibration problem. The objective of the installation was to install a multifunctional monitoring well with discrete sensors and distributed fiber optic cable as part of a CO2 sequestration demonstration project. Nevertheless, while monitoring each well completion, potential of characterizing each well completion process in terms of temperature anomaly and the feasibility of DTS as a monitoring tool of the well development process were investigated. However, since fiber optic cable was not calibrated before installation due to field schedule, we had difficulty understanding the data. Therefore, post-calibration methods to correctly correct temperature for more accurate interpretation was explored.

The uncertainty in depth calibration is difficult to reduce because the errors in depth are difficult to detect. In this paper, conventional depth calibration is applied by considering both stretching and wrapping of cable (Smolen & van der Spek, 2003). However, uncertainty in depth calibration was reduced as it could be confirmed with our gas lift temperature profile as it delineates known absolute casing depth.

The conventional temperature calibration method was applied by submerging both ends of fiber in ice or hot water to calibrate the temperature offset to absolute value and its rate of change along the fiber length (Smolen & van der Spek, 2003). However conventional method was limited to before installation and therefore not

always possible due to schedule on the field or other external factors. Therefore, post calibration method is proposed which considers the tight schedule on site and difficulty of submerging the long length in water after installation due to limited cable length. After installation, submerging fiber optic cable longer than laser pulse width is harder due to stiffness of the cable and other field challenges. The possibility of the two types of post-calibration methods are introduced for better practical application with accurately measuring rapidly changing temperatures and variations inside the well during completion.

Since the introduction to distributed sensing, DTS was used in many applications for down-hole monitoring such as optimization (Weaver et al., 2005), well integrity monitoring (Brown et al., 2000), real-time stimulation monitoring (Clanton et al., 2006), injection profiling (Brown et al., 2004) and gas lift and production monitoring (Fryer et al., 2005). While conventional uses of DTS to monitor gas lift and injection exists, we propose an alternate monitoring application of gravel packing and cementing process. Further, we have not yet found studies on obtaining and evaluating the entire well completion process. Therefore, we introduce DTS data of the entire well completion process from gravel packing to cement curing process. During well completion, real-time DTS data were used to optimize and overcome challenges during each process. The DTS data were analyzed to investigate and characterize temperature anomalies from each well completion process. As a result, each well completion process was able to be identified with distinctive temperature anomaly pattern. Consequently, observing the entire well completion process in real-time proved to optimize each well completion process and demonstrated to be an effective monitoring tool.

1.3 Outline

In this thesis, entire well completion is analyzed with DTS data including alternate application of gravel packing and cement curing process. However, before addressing the results obtained with DTS, basic fiber optic theory will be discussed including distributed sensing and how DTS decodes temperature in chapter 2. In addition, conventional depth and temperature calibration methods will also be discussed. In chapter 3, experimental settings will be mentioned with the necessary description of well completion process in interpreting the DTS data. The depth and temperature calibration methods used to interpret the DTS data will also be discussed in this chapter. In depth calibration method, the conventional method is applied but reduced uncertainty in depth calibration with the DTS gas lift data. In temperature calibration method, the post-calibration method will be discussed which was enhanced in terms of practicality on the field. Finally, analysis of the DTS data of complete well completion will be discussed including gravel packing, cement injection, gas lift operation, and cement curing. The optimization and effectiveness of monitoring the entire well completion process with DTS will be discussed.

Chapter 2. Theory

2.1 Basics of fiber optics

The optical fiber is a very thin silica structure that guides light along the length. There are three concentric layers to an optical fiber cable (Figure 2-1). The layers of the optical fiber are the core, cladding. The light pulses only travel through the glass of the core of the fiber and the cladding that has a lower refractive index than core act as a barrier to keep the light within the core. A small difference in the refractive index is enough to keep the light inside the core. The buffer layer is included for mechanical strength and protection. The buffer is extruded over the coating to increase the strength of the fibers further. The type of the fiber optic cable: multi-mode or single-mode fibers is determined by the size of the core (Fang, Chin, Qu & Cai, 2012).

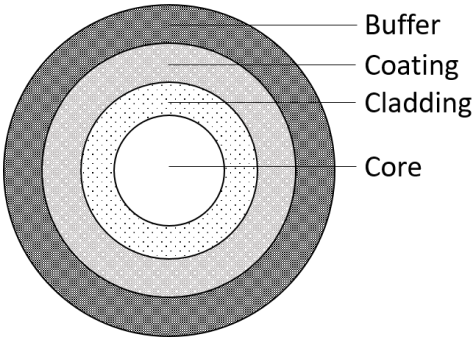

Figure 2-1. Schematic cross-section of a typical composition of the fiber optic cable (modified from Fang, Chin, Qu & Cai, 2012).

The single-mode fiber (SMF) has small light carrying the core of 8 to 10 μm. The small core allows only one mode of light to propagate which allows the light to travel to a further distance. The signal is able to travel further due to low attenuation as the number of light reflection created as the light passes through the core decreases in small core diameter. The light pulse traveling along the single-mode fiber is between 1300 nm to 1500 nm. The type of fiber is identified by the standardized colors on the outer jacket. The single-mode fiber has a green and brown color jacket and the multimode fiber has a blue and orange color jacket.

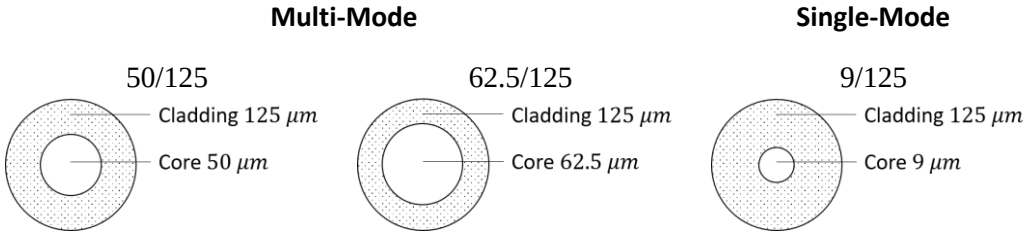

Figure 2-2. Configuration of multi-mode and single-mode cable.

The multi-mode fiber (MMF) has a large light carrying the core of 50 μm or larger. The standard size of the multi-mode core is 50 μm and 62.5 μm as displayed in Figure 2-2. The large core allows multi-modes of light to propagate but can only travel short distance due to fast attenuation rate. The large core increases the number of light reflections which allow more data to pass through but reduces the quality of the signal over long distances. The light pulse traveling along the multi-mode fiber is between 850 nm to 1300 nm. There are two types of multi-mode fibers: step index and graded index as illustrated in Figure 2-3. The step index is limited to sending a small amount of information due to some of the light ray traveling in direct route as oppose to zigzag travel as they bounce off the cladding. As different modes of light arrive separately, the aggregate of different modes begins to spread out, and the shape deforms. In order to prevent the shape from deforming,

overlapping of pulses need to be avoided by leaving spaces between pulses. The graded index is the type that is used in sensors because the light in the core curves travels helically making the distance the light travels shorter. The refractive index of a core determines the length of the core and diminishes gradually from center axis out toward the cladding. The light ray traveling helically has higher speed than the straight rays in the core axis, but both arrive at the same time because the core has a higher refractive index at the center than near the cladding (Crisp & Elliott, 2005).

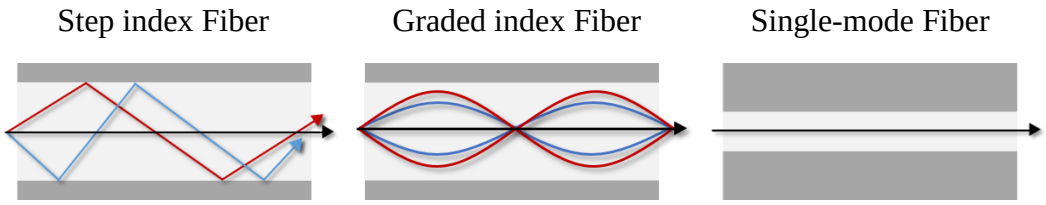

Figure 2-3. Modal distortion in multi-mode and single-mode cable.

2.2 Configuration of optical fiber sensors

The optical fiber sensors are classified into three different configurations: single point sensors, quasi-distributed sensor, and fully distributed sensors. The single point sensor has only one sensing point, and the sensor is usually at one end. Examples of single point sensor are pressure, strain sensors. The quasi-distributed sensor has multiple sensing points along the fiber, and they share the same interrogation unit. Therefore, a quasi-distributed sensor can measure different points of the location. The fully-distributed fiber optic sensors are a more advanced type of sensor as opposed to the point sensors and quasi-distributed sensor. The fully distributed sensor has a continuous sensing point along the fiber. Thus, the fiber optic cable itself acts as the sensor, and no additional transducers are needed. The interrogator sends pulses of light to the fiber and the interrogator measures the backscattered light. Scattering occurs in the fiber optic cable due to the inhomogeneity caused by changes in density, composition, molecular and bulk vibrations of the fiber medium. The fluctuation of the refractive index is due to localized variation density of the medium from the random ordering of the molecules. Therefore, spatial resolution can be changed because all part of the fiber responds to the measurand. It also enables continuous and real-time measurements along the entire length of the fiber optic cable (Wang, 2012).

2.3 Principle of scattering

The distributed temperature sensing is based on the OTDR principle. As the light pulse enters the fiber optic cable, the light is transmitted by total internal reflection (TIR) and at every reflection point, some of the light is backscattered in the form of elastic and inelastic scattering. Elastic scattering is when the frequency of the scattered light is the same as the incident light, and inelastic scattering is when the frequency of the scattering light would be shifted compared to the incident light (Figure 2-4). Three main types of backscattering occur simultaneously in fiber. The Rayleigh backscattering is elastic scattering, and Raman and Brillouin backscattering are inelastic scatterings (Fang, Chin, Qu & Cai, 2012).

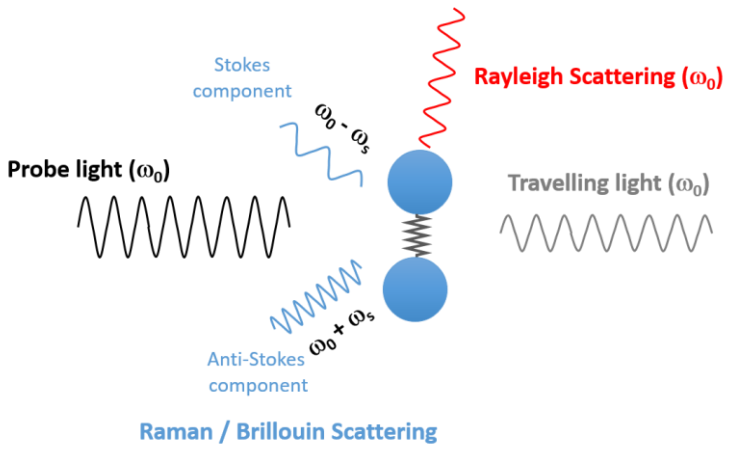

Figure 2-4. Schematic of backscattered spectrum with Rayleigh, Brillouin and Raman bands with anti-Stokes and Stokes component (after Kasap, 2013).

As Rayleigh backscattering is elastic, it does not divide into Stokes and anti-Stokes component. However, Raman and Brillouin backscattering are divided into Stokes component and an anti-Stokes component due to shift in wavelength. The anti-

Stoke component of Raman scattering, which has lower wavelength compared to Stokes component is sensitive to temperature, thus used in distributed temperature sensing. Although Brillouin scattering is sensitive to temperature and strain, it is not commonly used because it is difficult to separate from the Rayleigh band as it is too close. Therefore, the Rayleigh and Stokes signals are very weakly related to temperature and Rayleigh is sensitive to strain thus used in distributed vibration sensing (Fang, Chin, Qu & Cai, 2012).

2.4 Distributed temperature sensing (DTS)

The principle of distributed temperature sensing, DTS is based on the optical time domain reflectometry, OTDR. It measures the attenuation rate by launching light pulse down the fiber and analyzing the Rayleigh backscattered light. It measures the time and intensity of the backscattered light to correlate to the physical location along the fiber. As the light travels down the fiber, some light is absorbed into the glass and some leaks out of the fiber due to either imperfection in the glass or due to excessive bending of the fiber. If the attenuation rate is high, the signal may become weak due to light loss. It can measure the level of backscattering and detect small variations in the characteristic of fiber at any point in the fiber. It is generally used to measure overall loss, locate fiber breaks or faults, and detect gradual or sudden degradation of fiber and amount of signal loss at any point in an optical fiber. OTDR measurement is usually taken before and after installation to ensure the safety of the fiber (Fang, Chin, Qu & Cai, 2012).

The DTS uses the Raman scattering because the intensity of the Raman scattering is a function of temperature. When a short pulse is sent to the fiber, two distinct backscattering wavelengths is detected, which are the Stokes and anti-Stokes. During the collision of photons, the molecules vibration energy state can be changed. The Stokes scattering occurs when a scattered photon loses energy to the molecule and raise it to a higher vibrational-energy state. The anti-Stokes scattering occurs when a scattered photon gain energy by moving the molecule to lower vibrational-energy state (Brown, 2008). The Stokes scattering has a longer wavelength than the anti-Stokes scattering component. The amplitude and spatial localization of the backscattered light are determined with the propagation speed inside the fiber. The amplitude of the Stokes component is weakly dependent on temperature while the anti-Stokes component is strongly dependent on temperature.

Therefore, DTS measurement is obtained by the anti-Stokes component is very sensitive to the temperature (Wang, 2013).

The refractive index of the glass in fiber determines the velocity of light travelling inside the fiber. The wavelength of the light pulse launched into the fiber is within 800 to 1600 nm, which is in the infrared and visible spectrum. When the light enters the fiber, the velocity of light is slowed due to the refractive index of the glass in the fiber. The typical value used for the refractive index of the glass is 1.5, but it can range up to 1.7. The speed of light travelling down the fiber is 2×10^8 m/s and can be described by the following relation, where v is the speed of light inside the fiber optic, c is the speed of light and n is the refractive index (Smolen & van der Spek, 2003).

$$v = \frac{c}{n} \tag{2-1}$$

The light propagates through the fiber when the glass has a higher refractive index than the surrounding as the light is trapped inside the glass. The length of the light pulse, l_{pulse} is the travelling sensor moving through the fiber line. The length of the light pulse can be determined by knowing the pulse duration, t_{pulse}. The typical light pulse duration is 10 ns, which gives the length of the light pulse to be 2 m.

$$l_{pulse} = \frac{c}{n} \times t_{pulse} \tag{2-2}$$

The backscattered light return along the same path as the light pulse is travelled along the fiber making it a total two-way path length. The time window, t captures the backscattered light can be expressed as

$$t = \frac{2z}{v} \tag{2-3}$$

From the time of backscattered light received, the distance of the location can be determined. The time of the back scattered light must be measure in time sequence.

The light pulse launch repetition rate must also be considered because there cannot be two light pulses in the fiber at the same time. The light pulse must travel to the end of the fiber, and backscattered light must return before the next launch of a light pulse. Otherwise, the signals would be mixed and impossible to analyze the signal. Therefore, it is crucial to determine the minimum time between launches. The longer the fiber length, the longer time between launches.

$$t_{launch} = \frac{\left(2 \times d_{fiberlength}\right)}{v} \tag{2-4}$$

The typical launch rate is between 4000 to 10000 pulses per second. The higher number of pulses ensure better signal to noise ratio and better temperature resolution. In general, the resolution is improved proportionally to the root square of the number of samples, $\sqrt{n}$.

The DTS system consists of a laser light source, optical splitter, signal processing unit and a display unit as displayed in Figure 2-5a. The laser launches a short pulse of light down the fiber and travels through the pulse. The light is reflected along the boundary between the core and the cladding. The cladding keeps the light inside due to the difference in index of refraction and guides back to the center of the core. The scattered light is reflected back along the fiber toward the source, but a directional coupler separates the input laser light and backscattered signal. The backscattered signal is sent to a receiver where it filters out the Rayleigh and

Brillouin from the Raman backscattering signal. The backscattered light of the Raman component is then analyzed to determine how far down the fiber it originated by the intervals of the pulses. The spectrum of Rayleigh, Brillouin and Raman scattering is shown in the Figure 2-5b.

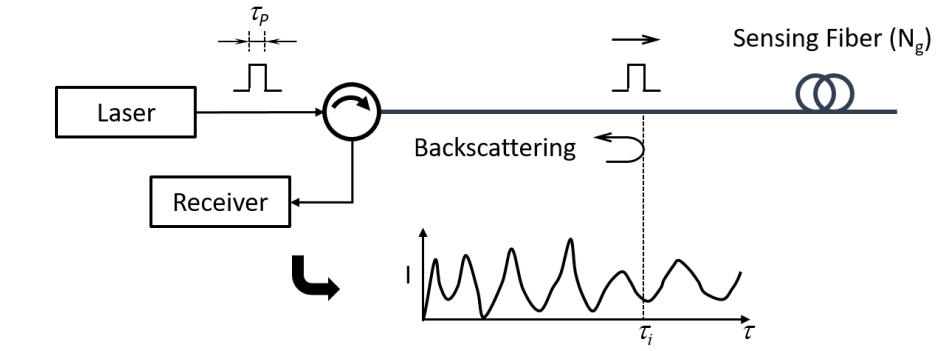

(a)

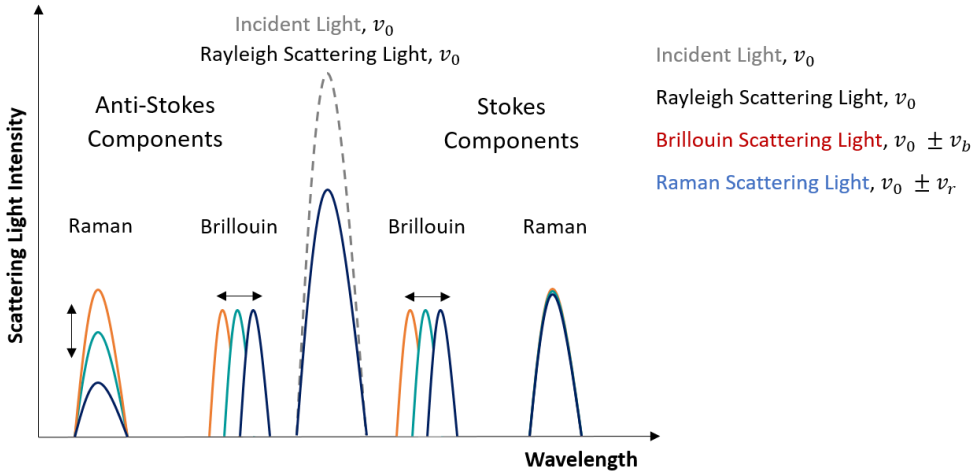

(b)

Figure 2-5. Schematic of (a) DTS system and (b) backscattering spectrum.

The performance of DTS acquisition system is characterized by spatial and temperature resolution. The spatial resolution determines the minimum distance to measure the change in temperature along the optical fiber. The temperature resolution determines the measurement time and depends on the launch repetition rate. Therefore, temperature resolution increases with the increase of sampling time (Silixa, 2016).

The acquisition time is used to set the averaging time of temperature signatures. Short acquisition times provide a better view of rapidly changing temperature signatures but have higher noise levels. Longer acquisition time improves temperature resolution due to averaging of noise, resulting in better the signal to noise ratio. The signal to noise improves approximately as the square root of the acquisition time. However, if longer acquisition time is used, we cannot obtain temperature signatures for shorter acquisition time. However, obtaining temperature signatures for longer acquisition time is possible by averaging short acquisition time temperature signatures (Silixa, 2016).

2.5 Temperature decoding

Once the light is back-scattered from the optical fiber, several components of different types of light information are given. The temperature decoding is possible using the anti-Stokes and Stokes components of Raman back-scattered light. The anti-Stokes component is sensitive to temperature and Stokes component is less sensitive to temperature. The intensities of anti-Stokes and Stokes component is displayed in Figure 2-6 with distance for the horizontal axis and intensity on the vertical axis. As the temperature change, Stokes component is linear with little change, and anti-Stokes change is more strongly defined (Wang, 2013).

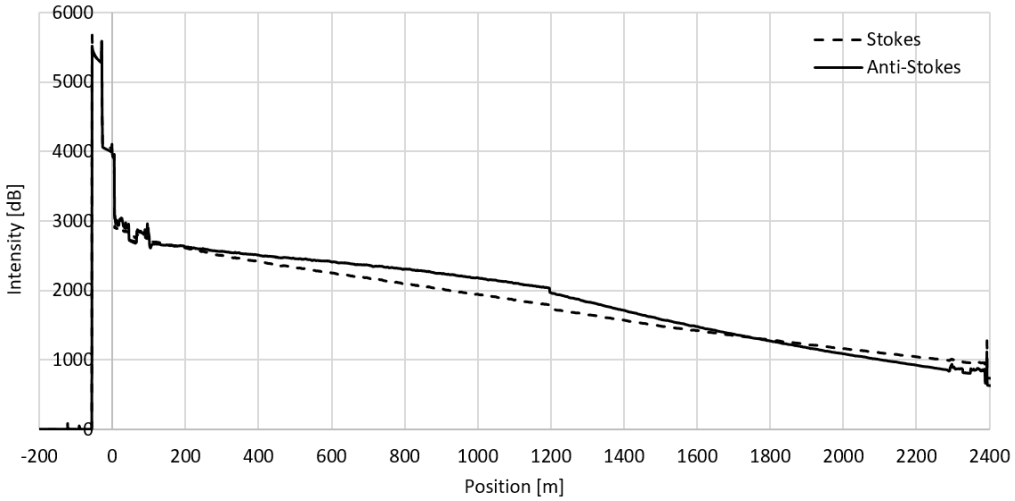

Figure 2-6. Comparison of the intensity change of anti-Stokes and Stokes components.

There are three different methods to decode the temperature using different components of the back-scattered light. The most commonly used decoding system is using both anti-Stoke and Stokes component of the Raman scattering. This decoding method is used with our Silixa's DTS acquisition system. The intensity of anti-Stokes light according to Wang (2013) is described as

$$I_a(z) = C_a x e^{-(\alpha_a+\alpha_r)z} \times R_a(T) \text{ , where } R_a(T) = \frac{1}{1-e^{-\frac{h\Omega}{2\pi kT}}} \qquad (2\text{-}5)$$

and the intensity of Stokes light is described as

$$I_s(z) = C_s x e^{-(\alpha_s+\alpha_r)z} \times R_s(T) \text{ where } R_s(T) = \frac{e^{-\frac{h\Omega}{2\pi kT}}}{1-e^{-\frac{h\Omega}{2\pi kT}}} \qquad (2\text{-}6)$$

The C_a, C_s are constants, $\alpha_a, \alpha_s, \alpha_r$ are attenuation factors of Stokes, anti-Stokes and Rayleigh lights within the optical fiber respectively, z is the distance, R is a function related to the local temperature, h is the Planck's constant, Ω is the shifted angular frequency and k is the Boltzmann constant.

To find the temperature signature equation, the ratio between anti-Stokes and Stokes must be found. By diving intensity of anti-Stokes over Stokes, local temperature profile can be defined as

$$\frac{I_a(z)}{I_s(z)} = \frac{C_a}{C_s}\, e^{-(\alpha_a-\alpha_s)z} e^{-\frac{h\Omega}{2\pi kT}} \qquad (2\text{-}7)$$

Equation 2-8 can be expressed in terms of temperature, which is defined as

$$\mathrm{T(z)} = \frac{\frac{h\Omega}{2\pi k}}{ln\left(\frac{C_a}{C_s}\right) - (\alpha_s+\alpha_r)z - ln\left(\frac{I_a(z)}{I_s(z)}\right)} \qquad (2\text{-}8)$$

The two other methods of decoding system are using only anti-Stokes component and using anti-Stokes component with Rayleigh scattering. There are both advantage and disadvantages of the decoding methods. The method of using only anti-Stokes component has no reference signals and may easily be affected by the variation of the laser source and filters. The method of using anti-Stokes and

Rayleigh may give a better signal to noise ratio due to a stronger Rayleigh scattering is used as a reference signal. However, it can be applied to only short to middle range and is easily affected by the variation by the fiber loss along the fiber. Although the method using a ratio of both anti-Stokes and Stokes component needs complex filters due to anti-Stokes signal being ten times weaker than the Stokes signal, it gives the reasonable accuracy of temperature measurements (Wang, 2013).

2.6 Calibration method

2.6.1 Temperature correction

The DTS measures the relative temperature value, not the absolute temperature value. Many DTS acquisition system has internal calibration system, however higher accuracy is needed for geoscience operating environment where the fiber optic cable may be under a condition of rapid change and large fluctuations in temperature. In the static condition, the calibrated temperatures are within ± 0.3 ℃, however under the rapid operating condition, the accuracy is increased to ± 2 ℃ (Hausner et al., 2011). The temperature measurement accuracy also declines as the length of the fiber is increased due to the power loss of the laser pulse (Smolen and van der Spek, 2003). The conventional correction method can be described with a simple case illustrated in Figure 2-7. The difference in temperature profile between the measured DTS data and absolute temperature data profile are clearly defined. In order to calibrate the measured DTS temperature data, offset and slope correction must be applied. The temperature correction can be done with two known points, $(d_1, T_1)\ and\ (d_2, T_2)$ as illustrated in Figure 2-7.

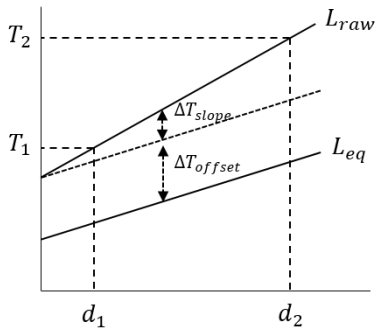

Figure 2-7. Diagram of conventional DTS calibration method where two points are known, $(d_1, T_1)\ and\ (d_2, T_2)$. The calibration can be done by correcting temperature due to slope, ΔT_{slope} and offset, ΔT_{offset}.

If the absolute temperature at two points are known, the theoretical equation of the absolute temperature line passing through both points can be found as defined in eq (2-9). The measured DTS temperature profile is denoted as L_{raw}, and theoretical temperature profile is denoted as L_{eq}. The temperature can be corrected by taking the difference due to slope, ΔT_{slope}, from every point of the DTS temperature profile, L_{raw} as defined in eq (2-10). After correcting the slope, the temperature needs to be further corrected by taking the difference due to offset from every point from slope corrected line as defined in eq (2-11). The order of slope and offset correction does not matter, however, finding the absolute temperature at two known points are crucial in calibrating the measured DTS temperature to improve the accuracy of the temperature value.

$$y - t_1 = \frac{(T_2 - T_1)}{(d_2 - d_1)} x - d_1 \tag{2-9}$$

$$T_{cor1} = L_{raw} - \Delta T_{slope} \tag{2-10}$$

$$T_{cor2} = T_{cor1} - \Delta T_{offset} \tag{2-11}$$

2.6.2 Depth correction

There are many areas where small errors can occur using the DTS system. The errors can arise from the instrumentation, the fiber, the nature of the installation, and other sources. These errors show up as depth discrepancies and temperature errors (Smolen and van der Spek, 2003). The depth issue is an unavoidable problem on the field, and unlike temperature correction, depth discrepancies cannot be pre-calibrated before installation. There are two inhibiting factors contributing to proper depth correlation between the true casing depth and the fiber length in-well. The first factor contributing to misleading depth is during installation, where the fiber optic cable coils around the casing. The second factor is the stretch of the fiber due to its own weight (Smolen and van der Spek, 2003). The percentage of the fiber optic cable stretch due to its own weight is defined as

$$s_w = \left(\frac{g\rho d_w}{E}\right) \times 100 \tag{2-12}$$

where g is the gravity constant ($9.8\, m/s^2$), ρ is the difference in density of glass and surrounding fluid ($0.4 \times 10^3 \frac{kg}{m^3}$), d_w is the well depth in meters, and E is the Young's modulus for glass ($70 \times 10^9 \frac{N}{m^2}$).

Before correcting the depth issue, the depth matching and the end of the fiber length need to be done. In dual-ended system or partially returned systems, the DTS data has a plane-symmetry where the right and left side are a mirror to each other. Therefore, if the DTS data is folded at the turnaround point, the data should be symmetrical. If the profiles do not overlay and events do not appear at the same depth, then the depth can be matched by determining the percentage of increase.

With the depth issue comes the issue of determining the end of the fiber depth. In a dual -ended system or partially returned, the end of the fiber is easily located with the peak and it can be confirmed with the raw data where splicing point has a sudden drop in temperature. Although it may depend on the application, Smolen and van der Spek (2003) states that generally ± 0.5 m is realistic for most application.

Chapter 3. Experiment setting with post-calibration method of temperature and depth

Thermal data were collected at Janggi basin, Pohang, Korea from well completion process to after well completion for further analysis. The thermal data were obtained from May 11, 2017 to June 13, 2018. The temperature data revealed processes of the well completion and delineating the events undergoing beneath the ground. Post-calibration method of the thermal data is tested with quality control of depth calibration.

3.1 Experimental setting

3.1.1 Study area

The thermal data were collected from Korea's first pilot-scale geological storage program at Janggi field which was launched in 2011. The Janggi field site is located at Pohang city which is the southeastern part of Korean Peninsula. The Phase I of the project was carried out from 2012 to 2015, which included site-selection and characterization of potential pilot-scale storage sites. The site selection procedure included finding the best candidate for reservoir formation with good porosity and hydraulic conductivity with caprock formation for sealing at a depth deeper than 800 m where the CO2 maintains supercritical phase. After several surveys, Janggi conglomerate, which is composed of clasts and the silty sand matrix was chosen to be the best candidate in terms of geological and hydrogeological perspective (Kim et al., 2018). The second phase was carried out from 2015 to 2017, which included in-depth investigation and characterization of target reservoir and caprock

formations by drilling seven boreholes. The geology at this site consists of conglomerate, mudstone, sandstone, and tuff formation.

The Janggi field site includes an auxiliary well, JG-7-1, monitoring well, JG-M, and an injection well, JG-I as illustrated in Figure 3-1. The monitoring well was completed at the end of May 2017. The thermal data were collected in the monitoring well, JG-M. The total depth, TD of the monitoring wells is 1092.44 m, and the well is slanted by 2 degrees. There is a 30 m thick Janggi conglomerate formation reservoir between 913.5 m to 960 m.

Figure 3-1. Location of Janggi field site including position of auxiliary, monitoring, and injection well.

3.1.2 Well schematic and completion process

The technologies deployed for monitoring purpose in JG-M with total depth, TD of 1192.44 m include 32-level ERT array, 24-level 3C geophone string, U-tube fluid sampler, 2 piezo pressure/temperature sensors (PT), gas-lift manifold for fluid production, experimental pH sensor, and distributed fiber optic sensor (DAS, DTS, heat-pulse). The schematic of Janggi JG-M monitoring well and the completion assembly employed during May 2017 operations is shown in Figure 3-2.

The 32-level electrodes were installed for performing ERT surface to the wellbore and cross-well imaging of the CO_2 plume. Due to 32 electrodes at the bottom of the well, almost all materials below 803 m are non-metallic or insulated for electrical resistivity tomography (ERT) measurements. Therefore, two types of casings, fiberglass reinforced pipe (FRP) and steel casing was installed in the JG-M monitoring well. The bottom 300.54 m used only 3-1/2 inch FRP casing and alternated between the slotted and non-slotted casing. The amount of slotted casing, which is labelled as three dash line in Figure 3-2, was chosen to allow adequate fluid circulation for gravel packing up to the level of the cementing stage tool at depth 909.94 m. Therefore, the boundary between FRP casing and steel casing is at 791.90 m.

The 3C geophones were installed for acquiring VSP data and passive micro-seismic monitoring. The 24-level geophone array was split into three strings, each containing 8-levels of 3C geophones to keep the overall size of the cable for insurance if one string fails during installation, not all geophones will be eliminated for sensing capability and to get to a workable diameter of the cable. The gas-lift manifold for fluid production installed at 605.55 m. The PT sensors were installed at the top and bottom boundary of the Janggi conglomerate formation, JGF reservoir

at 913.5 m and 960 m. The distributed fiber optic sensor turnaround was installed at 1082.56 m, at the second FRP non-slotted casing from the bottom.

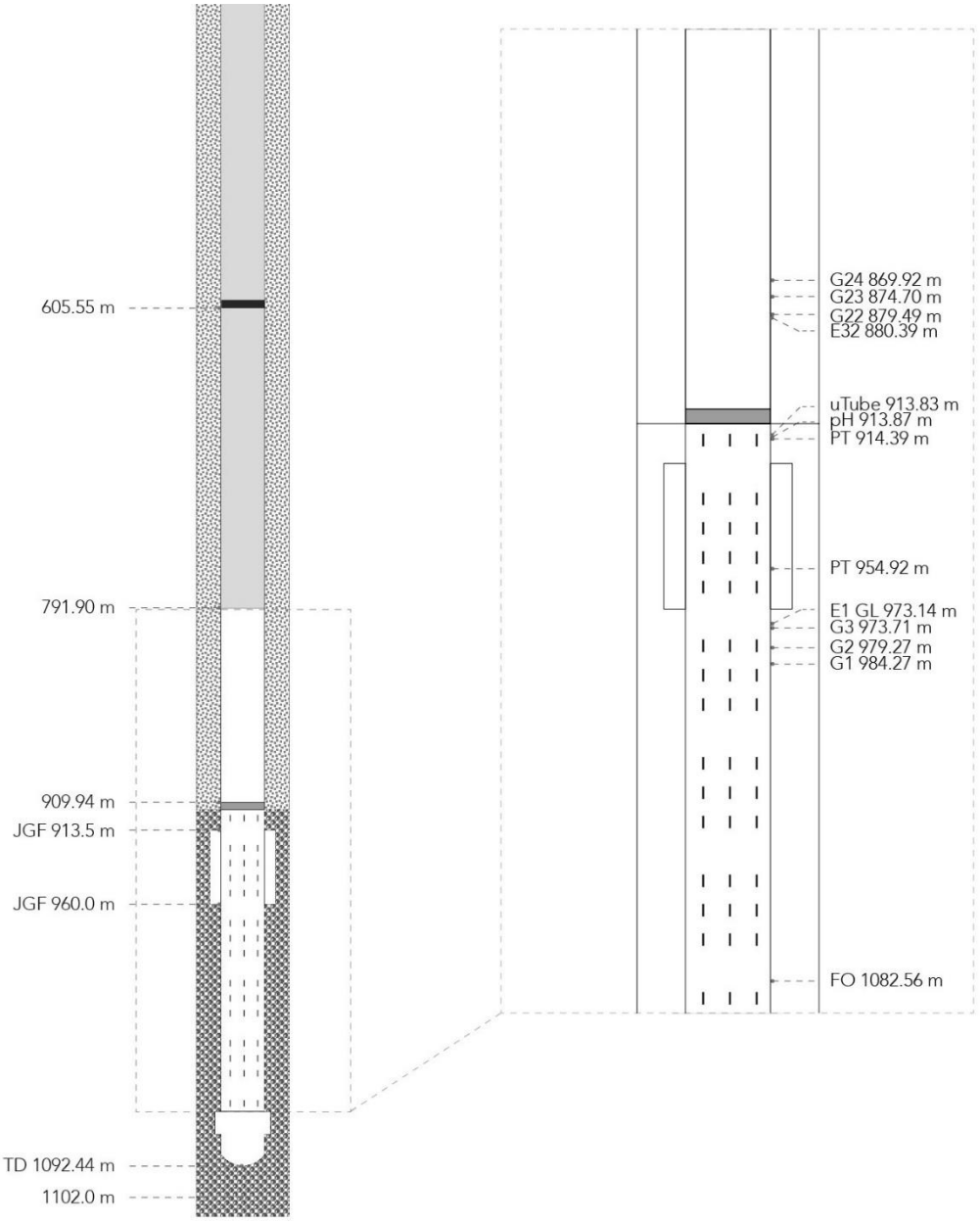

Figure 3-2. Schematic of monitoring well, JG-M and the completion assembly employed with gravel packing and cementing.

Series of centralizers and clamps were used to protect the cables during installation and good cement job as displayed in Figure 3-3. For FRP casing section, we used nylon decentralizer which were attached to the casing with 3/8 inch set screws. It was designed to push the FRP pipe to the side of the well to make room for the geophone pods that will be spaced at every 5 m. The mid joint clamp was used to hold the stainless-steel tubes. For steel casing section, the cannon cross coupling protectors with fins provide centralization during cementing and since every five joint was enough, cannon cross coupling protectors without fins were used in all the other joints.

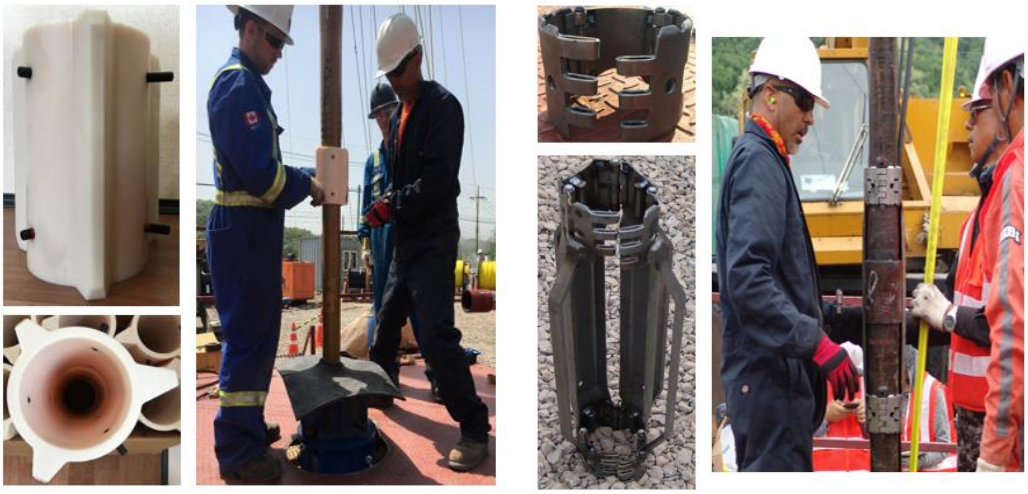

(a) (b)

Figure 3-3. Decentralizer and clamps used during installation (a) decentralizer for FRP casings (b) steel control line clamps for steel casings.

After landing the tubing hanger, DTS system and permanent pressure temperature gauge was used to monitor the process of gravel packing and cementing operation in May 2017. During gravel packing, the conventional method of using a packer for gravel packing was not used. Gravel packing was done without using a packer to ensure good coupling with the formation for VSP sensor. Instead of using a standard

gravel packing sand delivered down the tubing and using a crossover tool, 12/20 sand was directly injected in the annulus and recirculated the fluid up with the 1.9 inch IJ tubing. This method was a lot simpler than using a packer to isolate the gravel packed interval due to a large number of the line that would need to penetrate the packer system. After the gravel packing procedure, cementing of the bottom casing is conducted by circulating slurry into the well with the stage cementing tool at 909.94 m. The slurry was mixed in the hoper to remove the risk of plugging in the stage cementing tool. Then the wiper plug is pushed to the bottom because it will not fall to the bottom directly due to the friction of rubber fins and lack of fluid flow. The wiper plug is used to separate cement slurry from other fluids, which will reduce contamination and maintain predictable slurry performance.

An important aspect in terms of completion was to monitor the major steps during the completion of the monitoring well. The temperature profile of a well changes as the fluid is injected or withdrawn. The magnitude of these changes varies depending on different formation, injection time and rate, formation permeability and thermal properties of the fluid.

3.1.3 Fiber optic installation

There are four types of DTS installation, single point, single point with gauge, partially-returned single-ended, and permanent dual-ended installation as illustrated in Figure 3-4. The single point installation is just a straight fiber down to TD and single point with gauge, labelled as a dot in Figure 3-4 is an addition of an independent temperature measurement device. The semi-permanent installation is where the fiber is pumped partially uphole through a turnaround sub but not up to the surface. The dual-ended installation is similar to a semi-permanent installation, but the fiber reaches the surface. The turnaround sub is positioned at the lower point of temperature evaluation (Smolen and van der Spek, 2003).

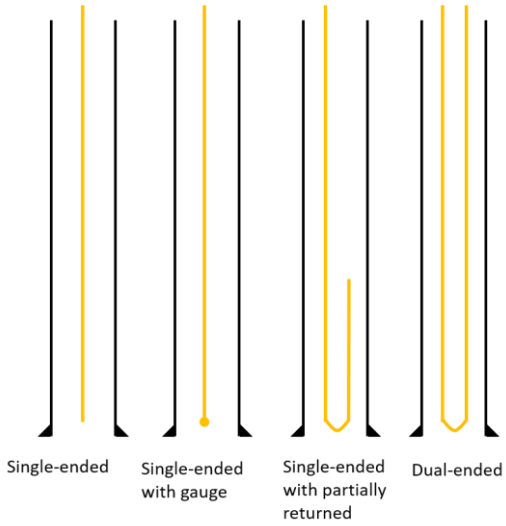

Figure 3-4. Fiber optic installation types including single-ended, single-ended with gauge, single-ended with partially returned and dual-ended.

In our Janggi field site, permanent dual-ended fiber optic turnaround sub was installed in the monitoring JG-M well. Although dual-ended system is more costly as it uses twice the length of fiber in the well, even in case the fiber breaks, the remaining fiber can be used as the partially-returned single-ended installation. Also,

the dual-ended system enables easier calibration even with non-linear attenuation. However, damaged fiber subjected to water is detrimental to fiber attenuation rate as water may remain in the capillary tube as the fiber is pumped with water. Thus the protection of fiber is crucial when pumping down the fiber optic line to prevent from scratches.

Inside the fiber optic turnaround sub, two types of distributed fiber optic sensing systems are contained within a single control line. Inside the control line, four optical fibers, which are two single-modes, brown and green and two multi-modes, blue and orange are looped together. The single-mode is used for distributed acoustic sensing (DAS), and multi-mode fiber is used for distributed temperature sensing (DTS). The fiber optic line is encapsulated with polypropylene for insulation and protection reasons. The fiber optic line used in Janggi basin has the following specification as illustrated in Figure 3-5. To monitor the CO_2 behavior, dual-ended fiber optic cables were permanently installed by tubing conveyed method and were permanently attached to the second lowermost non-slotted FRP at 1082.56 m. The turnaround was encapsulated in a potting compound, polypropylene for insulation and future protection inside a stainless-steel housing.

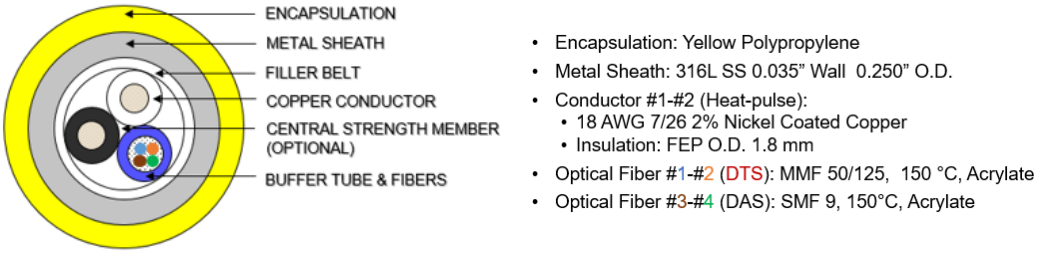

Figure 3-5. Fiber optic cable configuration types including (a) single, (b) partial turnaround, (c) dual-ended turnaround.

3.1.4 DTS configuration

In Janggi, Silixa's DTS interrogation system, XT-DTS along with installed fiber optic cable was used to monitor the temperature changes in observation well JG-M for five days during completion and monitoring curing for one month.

The data was obtained using a passive mode where no active heating was done to the cable itself. The interrogation unit was set to the sampling interval of 0.25 m with the acquisition time of 600 s during installation in May and 60 s in November to April. During installation, the optimal acquisition time of 600 s was chosen depending on accurate temperature signatures and low signal to noise ratio. From Nov to April, the short acquisition time of 60 s was chosen to see rapidly changing temperature signatures. The DTS measurement was continuously obtained in real-time to monitor the completion of the Janggi monitoring well. The uniform sampling enables us to track even the slightest changes in the wellbore and thereby to improve the understanding of the process taken inside the wellbore. The summary of DTS acquisition parameters used is shown Table 3-1.

Table 3-1. DTS configuration setting from May 2017 to April 2018.

	May - June	**Nov - April**
Sampling interval	0.254 m	0.254 m
Measurement length	2500 m	2500 m
Acquisition time	600 s	60 s

3.2 Depth correction

The location of splicing point inside the turnaround sub can be identified with raw Stokes and anti-Stokes data. In the anti-Stokes and Stokes data, the sudden drop in temperature marks the splicing point illustrated in Figure 2-6. In our data, the sudden drop in temperature has a range of 1 m from 1196.351 m to 1197.368 m as shown in Table 3-2. The maximum temperature drop is between 1196.606 m and 1196.860 m with 21.17 degree and second maximum temperature drop is between 119.860 m to 1197.114 m. However, considering our spatial resolution of 0.254, chosen the distance of 1197.114 m is close enough and is within 1 m distance range. Therefore, our chosen peak position of 1197.114 m was confirmed with the raw data.

Table 3-2. Distance vs anti-Stokes value from 1195.08m to 1198.131 m. The large difference in temperature denotes the splicing point.

Distance	anti-Stokes	Difference
1195.08	2032.78	
1195.335	2033.1	0.32
1195.589	2032.75	-0.35
1195.843	2031.67	-1.08
1196.097	2030.56	-1.11
1196.351	2028.78	-1.78
1196.606	2018.75	-10.03
1196.860	1997.58	-21.17
1197.114	1978.96	-18.62
1197.368	1971.27	-7.69
1197.622	1969.47	-1.8
1197.877	1968.88	-0.59
1198.131	1967.97	-0.91

Even though the cables were carefully dealt during installation to prevent little twist as much as possible during the installation process at the Janggi field site, cable coiling up around the casing, stretch of fiber optic cable itself, usage of decentralizer, and inner fiber optic twist may have contributed to the increase of total length of the fiber optic cable. In our Janggi field site, depth issue was not unavoidable and was found to be increased by comparing the depth between the casing length and cable line length as shown in Figure 3-6. The casing depth, D_c is 1082.56 m but the cable length, D_f is 1095.599 m, and therefore the difference in length, ΔD is 13.039 m. The length of the cable is increased by 1.2% compared to the casing depth and the DTS measures point in sampling interval of 0.254 m.

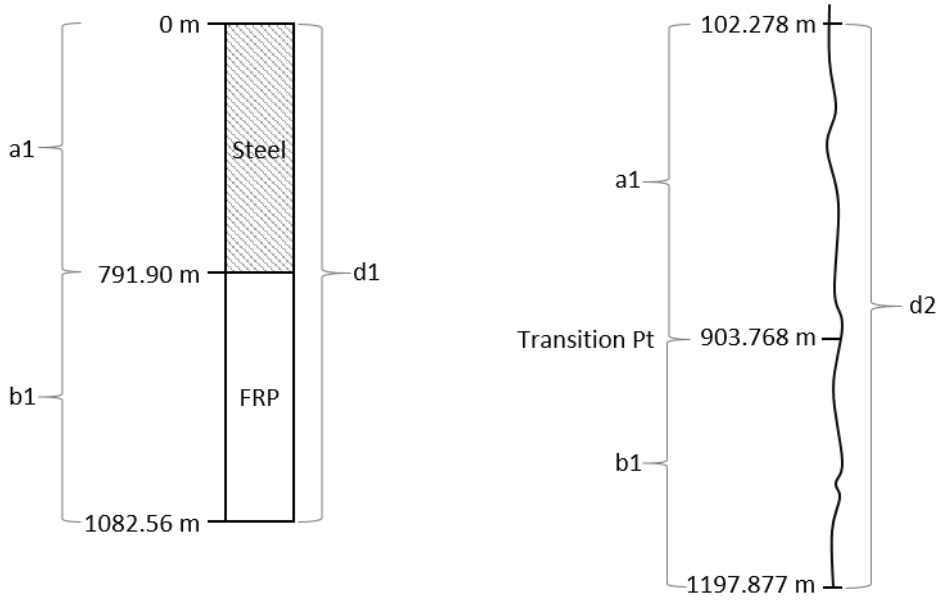

(a) (b)

Figure 3-6. Position comparison between casing and fiber optic cable where (a) is the casing depth and (b) is the fiber optic cable position on DTS system.

From installation, we know the casing depth is an absolute depth as there is no concern with winding or stretching. The known absolute depth is the fiber optic turnaround sub at 1082.56 m and the casing material transition point from FRP to steel is at 791.90 m. The depth issue can be confirmed from our gas lift data in both May and November as the location of the transition point from steel to FRP casing are clearly identifiable. This transition is displayed in thermal data as a difference in amplitude of the oscillation due to heat conductivity of the casing material by increased in temperature during gas lift process.

However, depth can be matched to the known position of the end of the fiber, which is the position of the turnaround sub, assuming that percentage of stretch is kept constant throughout. The depth can be calibrated using the known physical length, D_c and the number of points to the maximum peak, N defined as

$$\triangle d = D_c/\mathrm{N} \tag{3-1}$$

The redistribution gives sampling interval of approximately 0.251 and by using position, *x* in meters from DTS system, the calibration equation can be defined as

$$\mathrm{y} = 0.988465 \times x \tag{3-2}$$

The depth calibration data of the May and November gas lift process is displayed in Figure 3-7. After depth correction, the casing material transition point is within one-point difference, which is 0.254 m in terms of the DTS system's sampling interval to the true depth of 791.90 m. In both May and November, the difference to the true depth was 0.036 m. The 1.2% increase in length was redistributed throughout the total length by using the true location on the surface and the absolute location of the fiber optic turnaround at 1082.56 m. The large difference between

depth corrected and uncorrected data is due to the accumulation of the intervals, and therefore the difference increases towards the bottom.

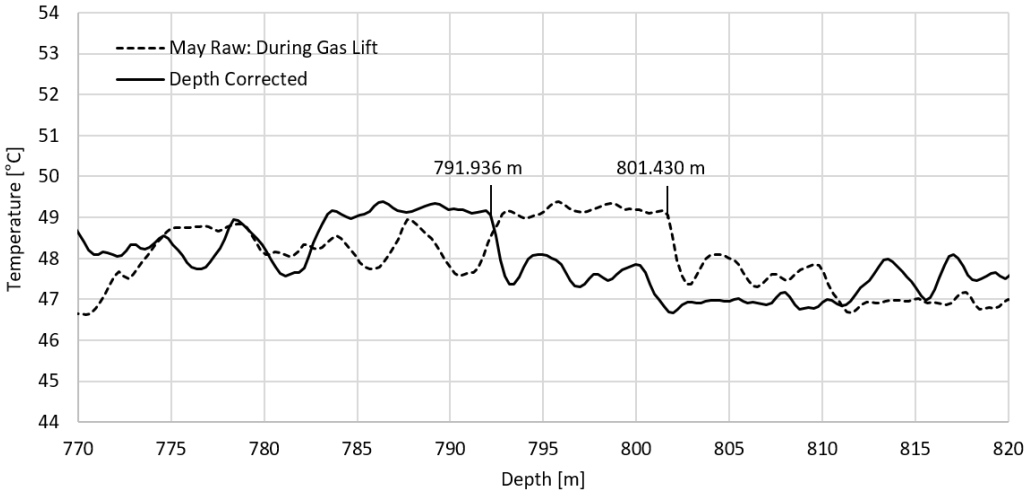

(a)

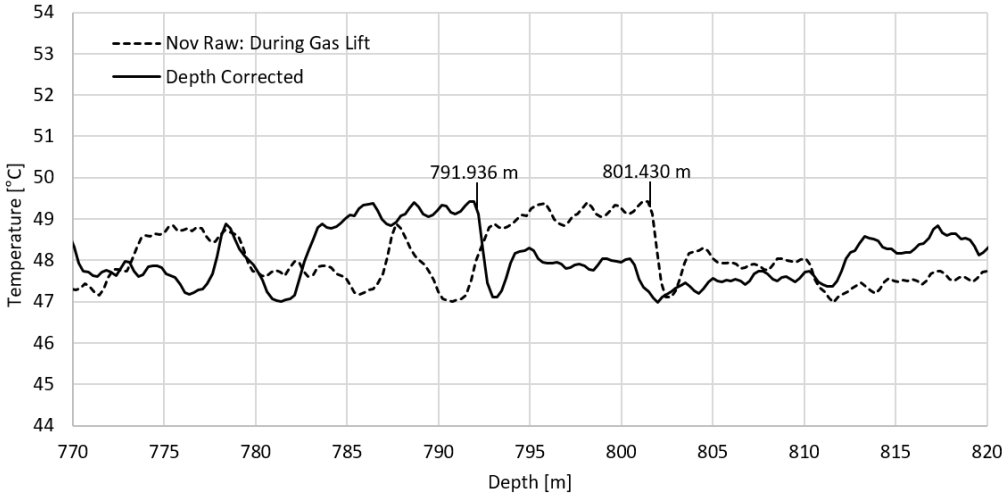

(b)

Figure 3-7. Before and after depth correction comparison with (a) gas lift data from May and (b) gas lift data from November.

Since the transition point from FRP to steel casing is known, the depth can be redistributed differently above and below the transition point and thus sampling interval applied differently in each section. However, the sampling interval turns out to be the same to the third decimal place with and without section division. Thus, no major improvement in depth calibration using section was seen.

After depth correction by redistribution, the transition point is within one-point difference, which is 0.25 m to the true depth of 791.90 m. The new sampling interval was applied to the cement injection data for verification and reliability of the depth correction. Although there is no known absolute position of the top of the gravel pack and bottom of cementing, the top of the gravel pack should be near 911 m and top of cement injection near 910 m. As mentioned in the installation section, there was 1 m spacing between gravel and cement injection for safety. Therefore, there should be approximately 1 m difference between the top of the gravel pack and the bottom of cementing. The depth correction result can be checked by applying the calibration to the cement injection data, which is shown in Figure 3-8.

In the cement injection data, the top numbers 913.259 m and 924.208 m indicates the top of the cement injection and were chosen right before the decrease of temperature. The difference to the expected top of the cement injection is 2.259 m which improved by 13.208 m before depth correction. The end of the cement injection temperature profile also delineates the top of gravel pack as the rate of injection of slurry is decreased as it permeates through the gravel pack. Therefore, once the slurry meets the gravel pack, it will permeate slowly and its temperature effect will not be immediately displayed. The bottom numbers 912.003 m and 922.937 m indicates the top of the gravel pack and were chosen at the point right after the last drop in temperature. Thus the final bottom of the slurry will display later in the temperature profile as the temperature will change more slowly. The

difference to the expected top of the gravel pack is 2.003 m which improved by 12.937 m before depth correction. Since both top of cement injection and top of gravel pack is near our expected depth, we can safely assume that redistribution displays more true depth representation of the well.

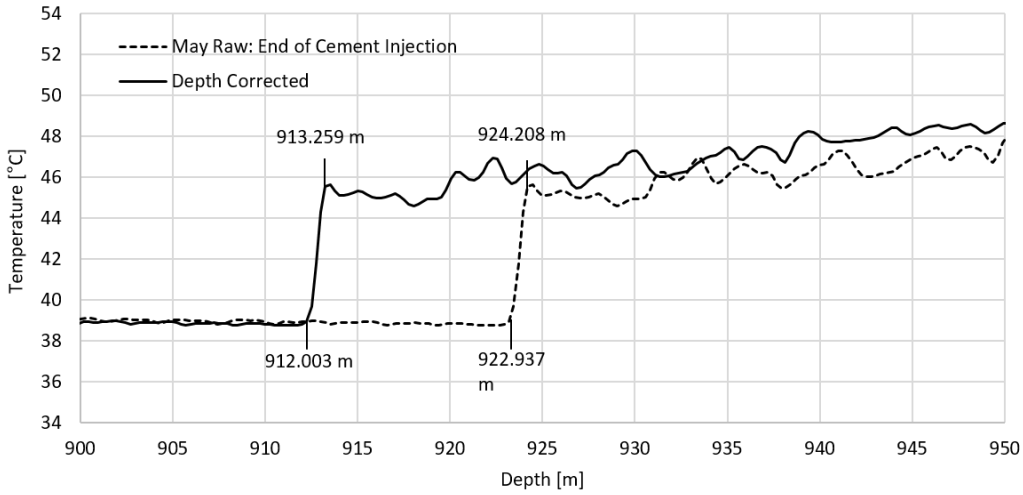

Figure 3-8. Before and after depth correction comparison with end of cement injection data from May.

There are several reasons why the DTS measures depth longer. The change in DTS system sampling interval of the third decimal place may increase the total length. Even with the sampling interval differences, already there is about 13 m difference in depth. Another factor to think about is the winding of the fiber optic cable during installation. At our site, 113 88.9 mm casings were used and if only one tenth of winding of cable occurs for each casing, there is about 3 m difference in length. There are many factors to the total length increase thus depth calibration is crucial to understanding the DTS data.

More precise depth calibration can be done with more known points in the well, and thus more accurate percentage of the winding can be found. Therefore, obtaining well logging data before installation is a good idea because it can be used as a reference data for calibrating the DTS data. Although the DTS is the more superior form of acquiring thermal data, as once installed, it can measure temperature anytime, calibration must be done before using such data, and that can be done with the well logging data. The depth correction can be improved by knowing more points in the well as more winded section can be determined. Therefore, obtaining a well logging data is a good idea before well completion to use for correction data for DTS data.

3.3 Temperature correction

In our experiment, pre-calibration could not be done prior to installation, therefore we suggest post-calibration method that is within the acceptable range of error, 0.3 ºC. The necessity of temperature calibration of DTS data is mentioned in the previous section. Figure 3-9 depicts the problem of DTS data between before and after temperature calibration of DTS data. In dual-ended fiber optic installation, the left and right side of the data should be a mirror to each other. The left and right side of the peak should have the same temperature. However, without calibration, due to optical power loss, the end point on both side do not equal as displayed in Figure 3-9.

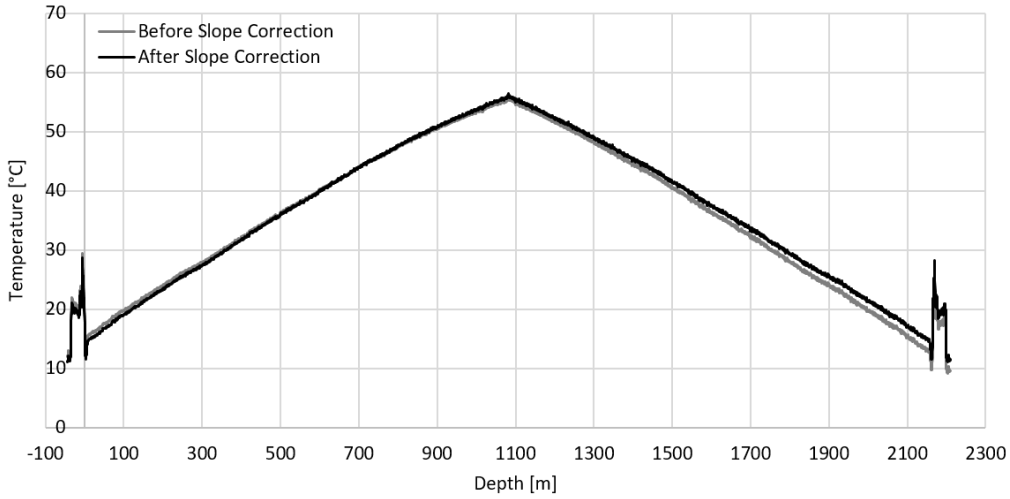

Figure 3-9. Comparison between before and after temperature correction is displayed in gray and black respectively.

In this section, post-calibration methods are explored as obtaining an accurate absolute value temperature is an important factor in a post-calibration method. The necessary steps to finding more accurate absolute temperature values will be explored. Therefore, three experiments were done to find the best temperature calibration methods of post-calibration.

Three calibration methods were tested and compared the effectiveness of each method in borehole JG-M in April 2018. The experimental setting at the Janggi Field site is displayed in Figure 3-10. The “water tub” is the conventional method of correction by submerging about pulse width length of fiber optic cable in water to find the stable absolute temperature. Even though it is best to submerge the fiber optic cable in water for temperature correction, this may not always be possible due to difficulty in submerging length of pulse width in water once it is installed. Therefore, a pointwise method of correction using a heat coil is suggested by heating fiber optic cable near the well with heat coil. The “diver” is another pointwise method of correction by using the position of heat coil to apply slope correction and using the absolute temperature value inside the well to apply the offset correction. For all cases, the slope correction was applied to temperature profile with no events in the well, and background temperature data was collected for 15 min before the calibration method experiment. Table 3-3 summarizes the calibration experiments done in April 2018.

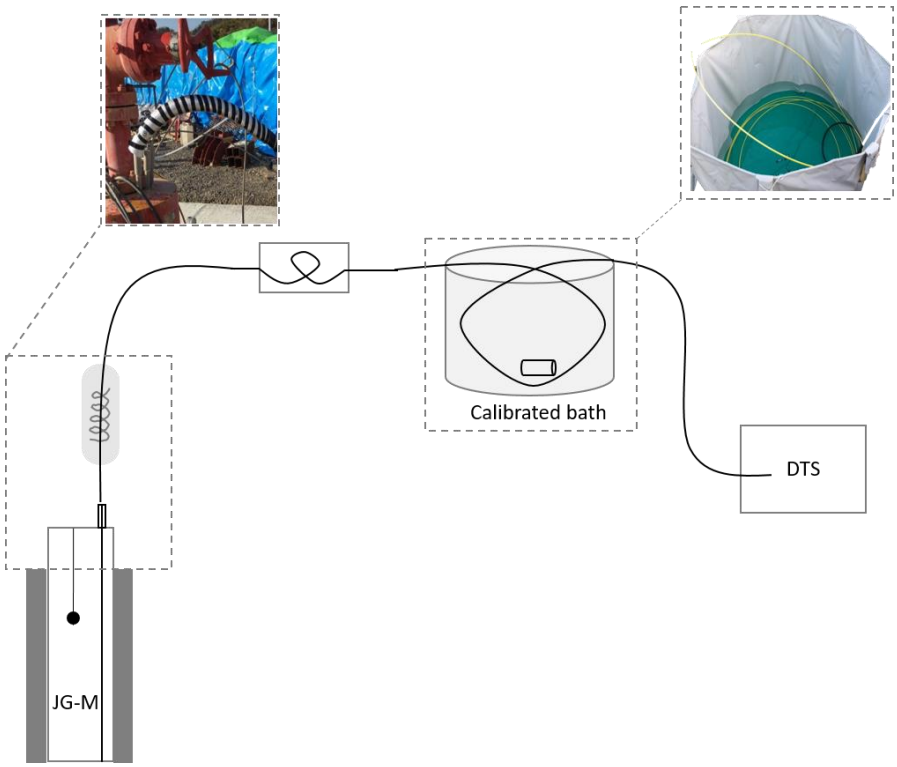

Figure 3-10. Calibration experiment setting with diver represented as a solid black dot inside the well, heat coil wrapped around the fiber optic cable outside the well, and calibrated bath.

Table 3-3. Summary of DTS calibration events.

Test #	Event	Date	Start time	End Time	Remarks
	Background	April 11	14:10	14:25	
1	Heat coil	April 11	14:26	15:02	Temperature effect lasts till 17:30
2	Water tub	April 11	15:45	18:50	
3	Heat coil	April 12	9:29	9:48	Temperature effect lasts till 10:15
4	Diver	April 12	10:35	11:35	

3.3.1 Post calibration method

The temperature calibration method mentioned in the theory section can be applied in single-ended fiber optic installation. In Janggi field, dual-ended fiber optic cable is installed, and an example of dual-ended DTS data is displayed in Figure 3-11. In a dual-ended configuration, the accuracy of temperature decreases on the right side due to power loss, resulting in misleading temperature values. The dual-ended calibration is similar to single-ended calibration. However, in dual-ended calibration, only one point of absolute value is needed because knowing one point results in having two points in dual-ended system. In dual-ended, the fiber is returned at the bottom of the turnaround sub; thus the endpoint returns to the surface. Therefore, if the fiber is spread out, then two points are known as displayed in Figure 3-11. There are two types of temperature calibration, the slope and offset correction. Conventionally pre-calibration of the fiber optic cable before installation must be done to obtain accurate temperature value. However, the calibration can be done after obtaining the data by post calibration method.

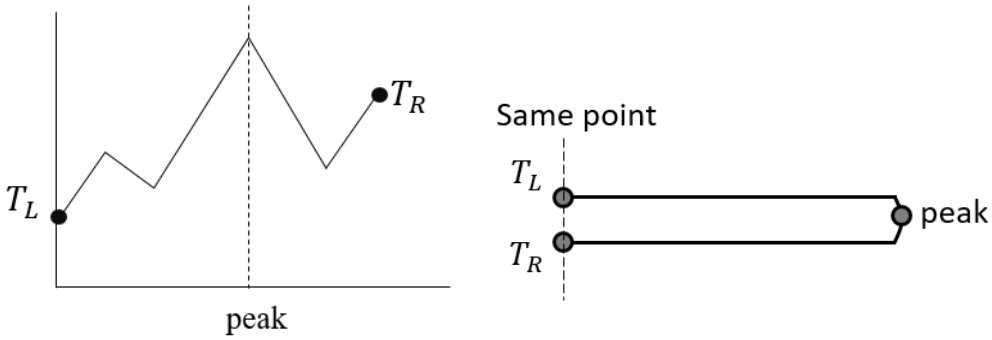

Figure 3-11. Example of DTS data before temperature correction.

The first step to calibrating the temperature is to find the theoretical equation of a line (slope and intercept) passing through the two testing points. The theoretical equation, T_{eq} can be defined as

$$T_{eq} = m * x + b \tag{3-3}$$

where m is the slope or temperature gradient, x is the position of raw DTS data in meters, and b is the intercept value of a temperature. Then theoretical temperature at each sample points are calculate and the difference to the measured value, T_L is found. The difference equation is defined as

$$\Delta T = T_L - T_{Eq} \tag{3-4}$$

where T_L, is the true temperature value and T_{Eq}, is the theoretical temperature value. The corrected temperature, T_{cor1} is defined as

$$T_{cor1} = T_{raw} \pm \Delta T \tag{3-5}$$

where, T_{raw} is the measured DTS temperature value and T_{diff} is the difference between the true and theoretical temperature value. The slope equation depends on the direction of slope and T_{raw} is either added or subtracted to T_{diff} as shown in Figure 3-12. If the slope is negative, T_L has higher temperature value than T_R, therefore the temperature has to be shifted upwards. If the slope is positive, T_L has lower temperature value than T_R, therefore the temperature has to be shifted downwards. After slope correction is applied to the DTS data, offset correction is applied to shift the temperature to the measured absolute temperature. The offset temperature correction is defined as

$$T_{cor} = T_{absolute-diff} \pm T_{cor1} \tag{3-6}$$

where $T_{absolute}$, is the difference of the physically measured absolute temperature and slope corrected temperature value and the T_{cor1}, is the temperature with the correct slope.

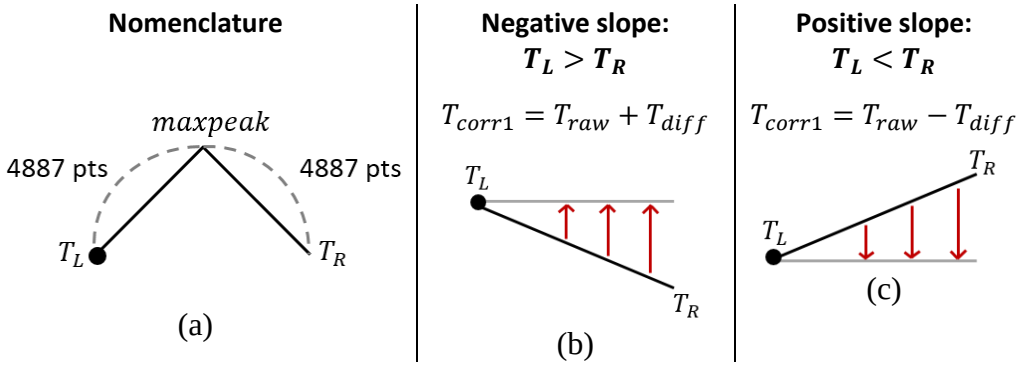

Figure 3-12. The slope equation depends on the direction of the slope, where (a) is the nomenclature, (b) is the negative slope, and (c) is the positive slope.

3.3.2 Long point calibration method with water tub

In the water tub experiment, the fiber optic cable was submerged in water for 22 m, which is more than pulse width length of a laser. The temperature stabilizing in the calibrated bath, water tub experiment is shown in Figure 3-13. The water tub experiment was carried out for about 3 hours and it took 1 hour for 22 m of fiber optic cable to reach to a stable temperature on the DTS data. The time it took for the temperature to stabilize, and temperature decreasing, and the length of the cable submerged can be seen in the DTS data displayed in Figure 3-13.

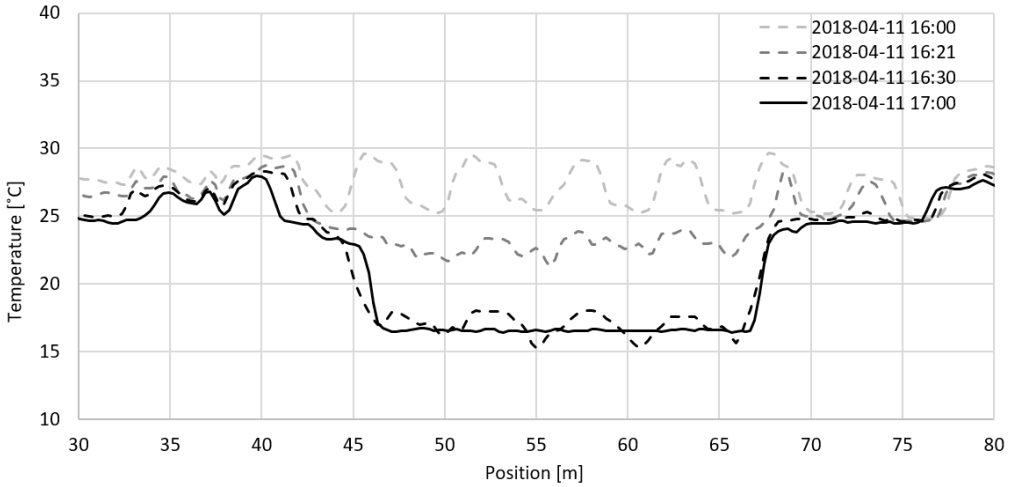

Figure 3-13. Time progression of DTS data of fiber optic cable submerged in water.

For water tub calibration method, data when the water tub data has stabled from 2018-04-11 17:37 to 18:49 were used. After the temperature stabilized (4/11/2018 17:00), the position of the cable submerged in water could be clearly seen on the left and right side of the DTS data, due to dual-ended installation of fiber, as shown in Figure 3-14. The left side of the data ranges from 48.896 m to 64.148 m, and the right side of the data ranges from 2329.826 m to 2345.078 m. Since the submerged

part of the fiber optic cable must have the same temperature, the inner 60 points were averaged to eliminate fluctuation of the temperature value on each side. The middle point on the left side was at 56.522 m, and middle point on the right side was at 2337.706 m. To make sure the right middle point matched the left middle point, same number of 4887 points to max peak were used.

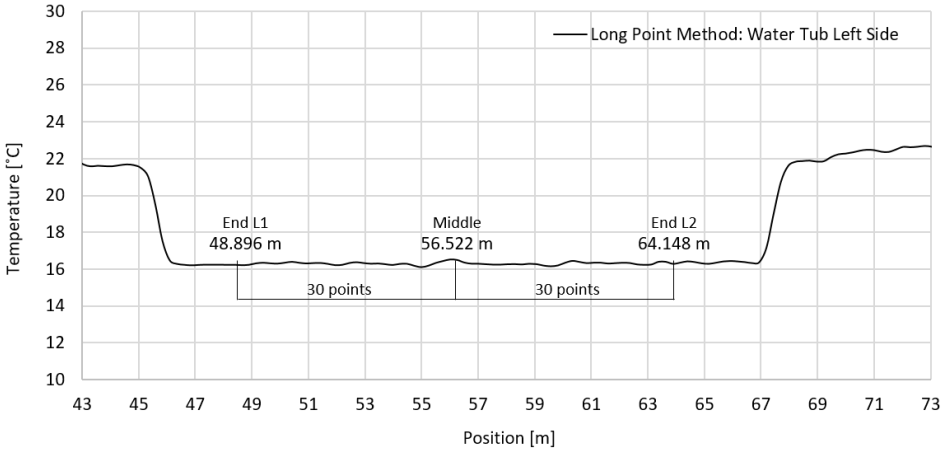

(a)

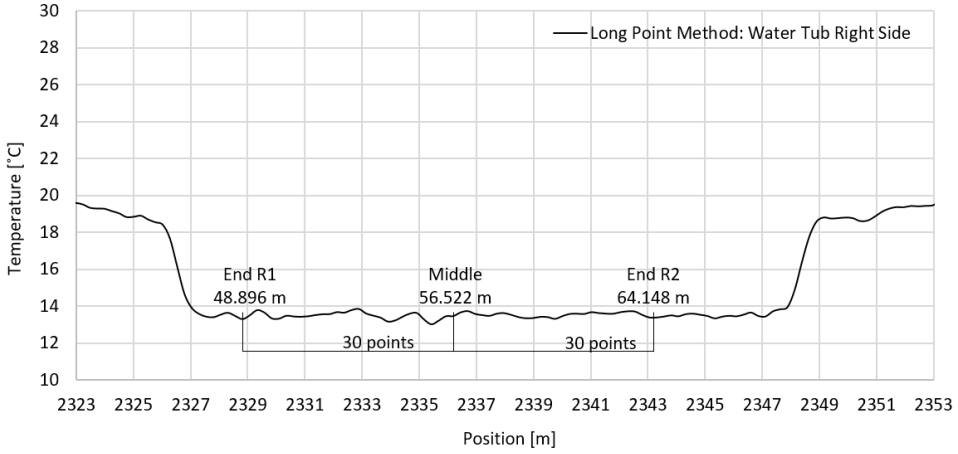

(b)

Figure 3-14. Locating the middle point of submerged fiber optic cable in water tub (a) on the left side and (b) on the right side. The range of average temperature value is shown as well.

In order to find a better slope correction factor, the temperature change of water within an hour was considered. Even though the specific heat of water is lower than air, the minimum difference between the left averaged temperature value and right averaged temperature value data was considered for better estimation of the reference temperature. The ten-minute range which gave the minimum difference between the left and right averaged temperature data is 17:53 to 18:02. From the best ten minute range, the minimum, maximum, and average slope value was used to find the slope equation. The maximum slope gave the minimum difference between left, and right value. The minimum slope gave the maximum difference between left and right value. The water tub temperature calibration tests are summarized in table 3-4. The slope curve of minimum, maximum and average slope is shown in Figure 3-15a. In the table, "all" represents using all the data points without considering the temperature change of water, "DTS" represents the best ten minute data in terms of minimum difference between left and right endpoints, and "diver" represents the most stable temperature measured with the diver in the water tub for ten minutes.

Table 3-4. Summary of water tub temperature calibration test.

	All No Avg.	**All 60pt Avg.**	**DTS No Avg.**	**DTS 60pt Avg.**	**Diver No Avg.**	**Diver 60pt Avg.**
Diff Min	2.463	2.731	2.490	2.777	2.517	2.766
Diff Max	3.169	2.974	3.145	2.868	3.169	2.954
Diff Range	0.706	0.243	0.655	0.091	0.652	0.188
Diff Average	2.828	2.837	2.806	2.810	2.902	2.854
Slope Min	-0.0013892	-0.0013037	-0.0013787	-0.0012572	-0.0013892	-0.0012950
Slope Max	-0.0010797	-0.0011973	-0.0010915	-0.0012174	-0.0011034	-0.0012125
Slope Range	0.0003095	0.0001063	0.0002871	0.0000398	0.0002858	0.0000825
Slope Average	-0.0012399	-0.0012437	-0.0012301	-0.0012320	-0.0012722	-0.0012511

The “DTS” method gave the best result where 60 points were averaged to eliminate fluctuation of the reference temperature, and the slope curves are displayed in Figure 3-16a. This was confirmed again by comparing all three methods as displayed in Figure 3-15. The averaging of 60 points to eliminate fluctuation of reference temperature was the most effective in all three cases as it had smaller slope and difference range. In order to apply the slope equation, it is best to apply to the data without any events. Therefore, background data from April 12 before any experiment was used for all three cases in the post-calibration method. The left end point, T_L is the true temperature as the left side of the max peak is more sensitive to temperature. The temperature accuracy improved after temperature correction, as the difference to true temperature decreased from 2.6 ºC before correction to 0.02 ºC.

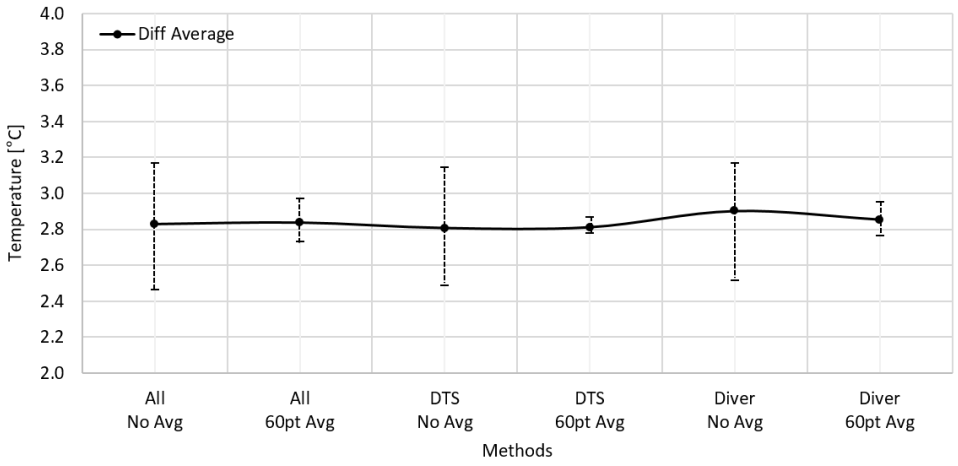

(a)

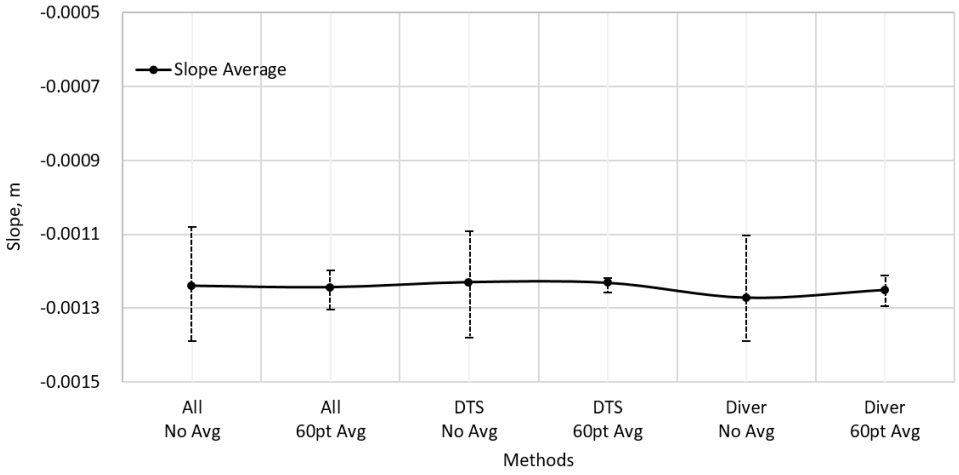

(b)

Figure 3-15. Comparison of long point water tub methods in terms of (a) slope range and (b) temperature difference.

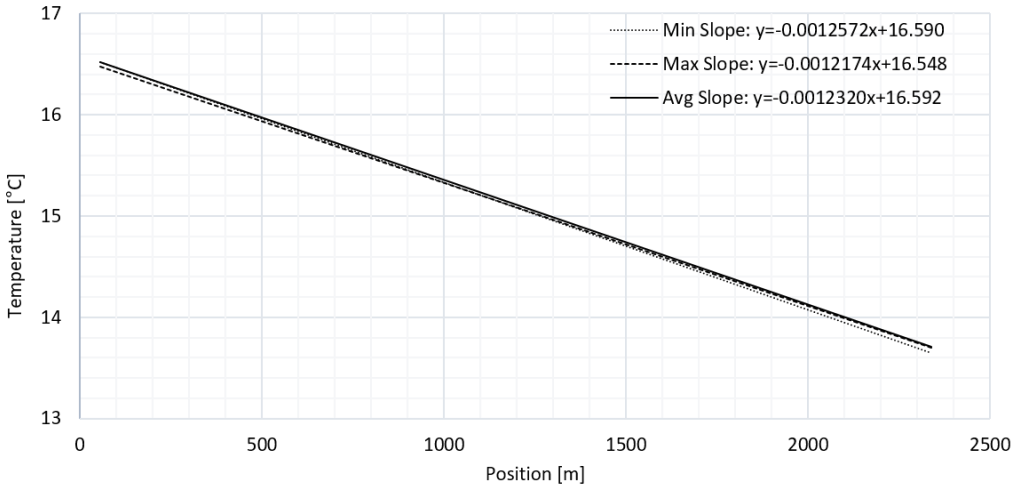

(a)

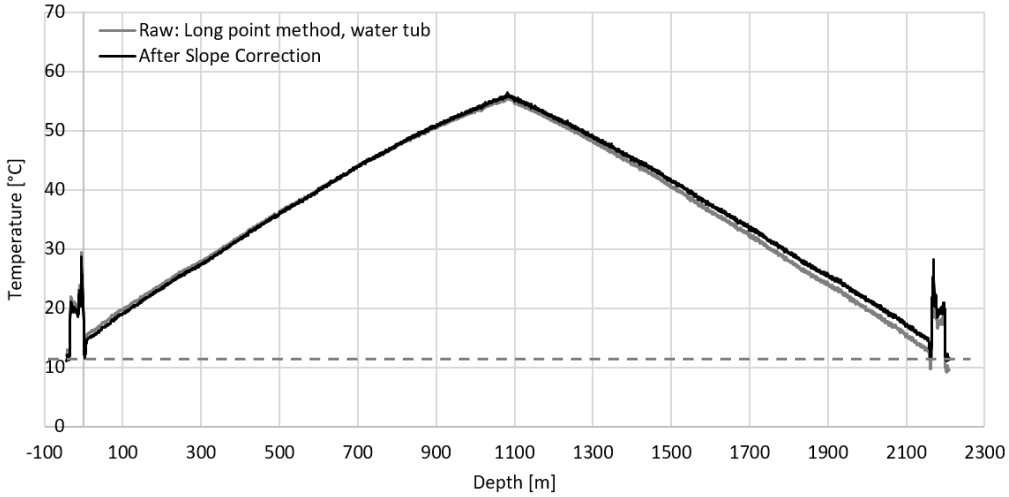

(b)

Figure 3-16. (a) Slope curve of long point method with best 10 minute range of DTS 60 point average from 17:53 to 18:02 and (b) heat profile after long point water tub temperature correction.

3.3.3 Point-wise calibration method with heat coil

The point-wise method with heat-coil calibration experiment was carried out after the long point water tub experiment. The heat-coil was used to locate the position on the DTS data for slope correction. The heat coil of 0.5 m in length was wrapped around the fiber optic cable near the well and insulated with a sponge tube of 1.5 m and taped around to keep the temperature from fluctuating from the wind as shown in Figure 3-10. The distance from the middle of heat coil to the well was 70 cm. In heat coil experiment, obtaining the absolute temperature value was difficult as the temperature could not be stabilized. Therefore, the ambient temperature value at the heat coil position was used for slope correction. On April 12, the fiber optic cable was heated with heat coil to about 50 degrees for about 10 minutes and observed the cooling for 27 min. The heat coil position recorded on DTS data was at 101.7 m on the left side and 2293.475 m on the left side as illustrated in Figure 3-17.

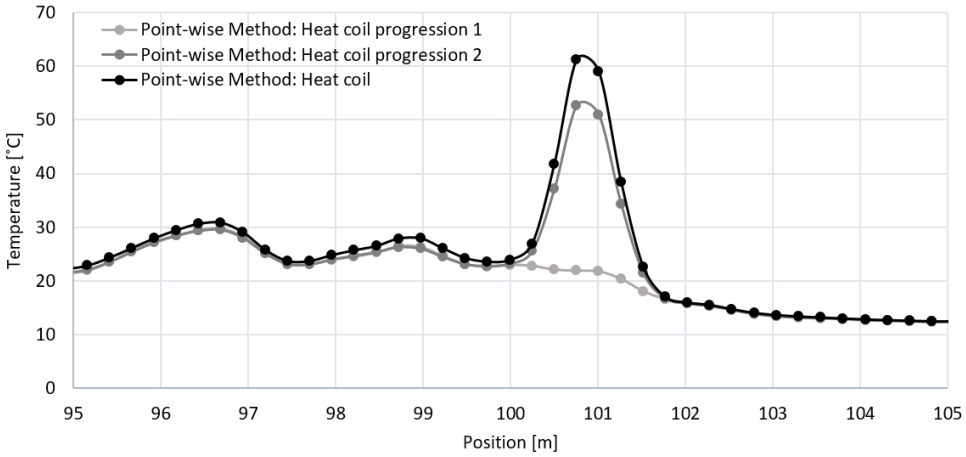

(a)

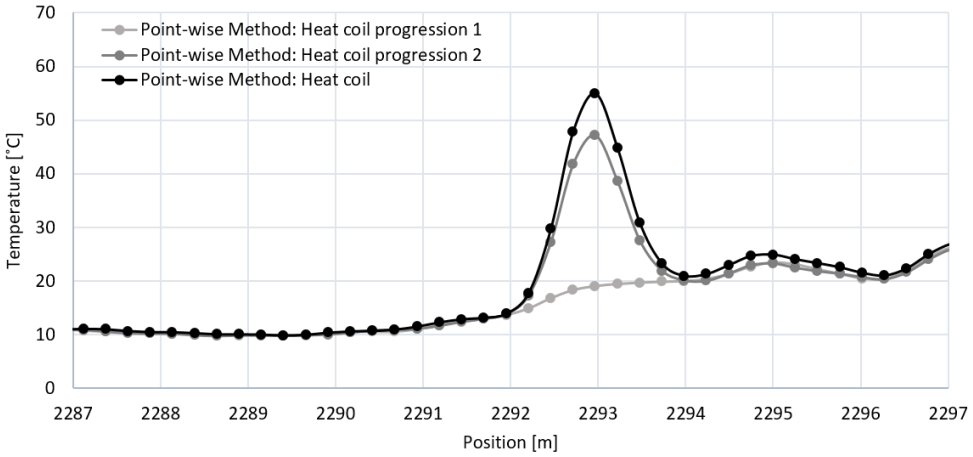

(b)

Figure 3-17. Heat coil position recorded on DTS data (a) on the left side and (b) on the right side.

The slope curves are displayed in Figure 3-18a and the slope equation is very different from the long point water tub method. In this case, because the absolute temperature is not known, only slope correction was applied. Even with only slope correction, whether the calibration is done correctly can still be evaluated by comparing the two endpoints. After applying the calibration to the data, the two

endpoints on the left and right need to have the same temperature value. However, Figure 3-18b which display the heat profile with point-wise heat coil slope correction showed incorrect calibration. Even though there is an improvement of 1.1 ºC to true temperature after correction, the left and right endpoints still has 1.5 ºC difference.

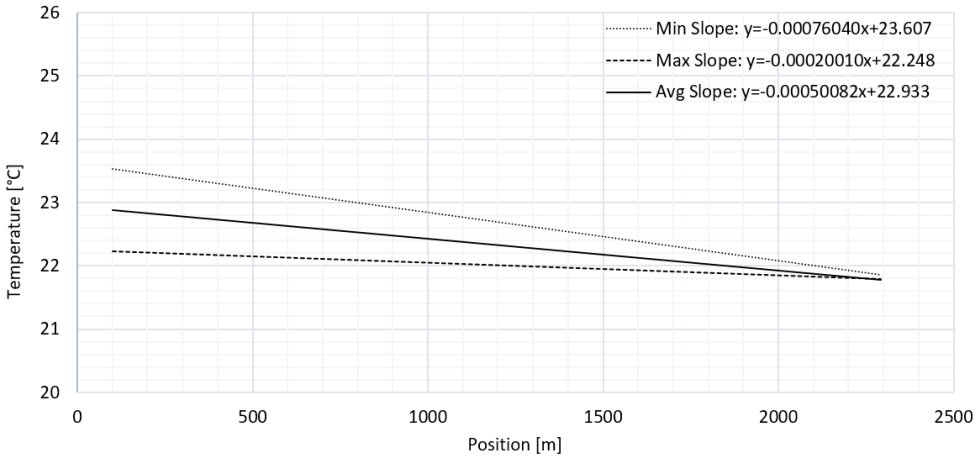

(a)

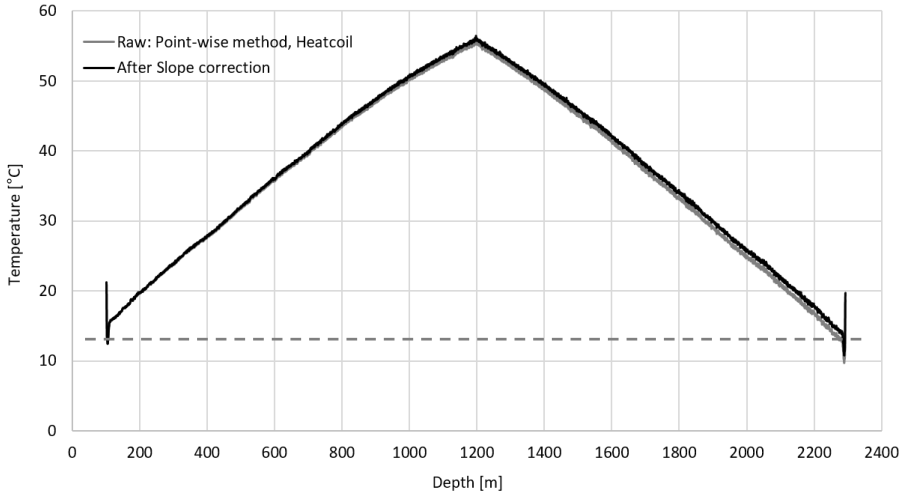

(b)

Figure 3-18. (a) Slope curve of point-wise method with heat coil and (b) heat profile after point-wise heat coil slope correction.

3.3.4 Point-wise calibration method in-well

After confirming the failed case of the point-wise method of using only the heat coil, it was decided that the problem was not using point-wise but obtaining temperature value on the surface. On the surface, air temperature is quickly affected and has higher than specific heat constant than water. Thus diver was lowered into the well at 10 m, 20 m, 30 m to obtain absolute value temperature. The diver position on the DTS could be located by counting from the known heat-coil position. The position could also be confirmed because when the fiber optic meet in-well water, the temperature profile shows a decrease in temperature. Also, it was only 1 m to in-well water from the heat-coil position.

The slope curves found with the point-wise in-well method is similar to long point water tub method as displayed in Figure 3-19. The slope curves did not improve as the diver went further deep into the well; instead, all three position gave similar slope curves. Although the slope curves are not as close to each other as the long point method, it gave a reasonable temperature correction as displayed in Figure 3-20. After temperature correction with point-wise in-well at 10 m, the temperature accuracy improved as the difference to true temperature is only 0.06 ºC compared to before temperature correction, the difference to true temperature was 2.8 ºC.

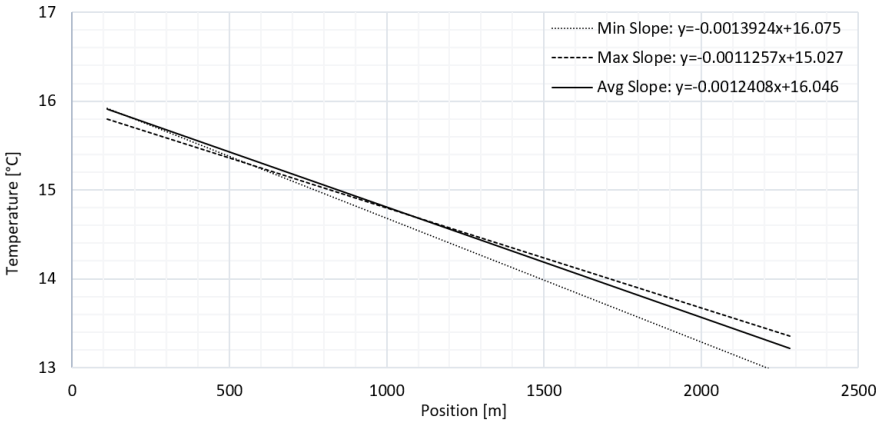

(a)

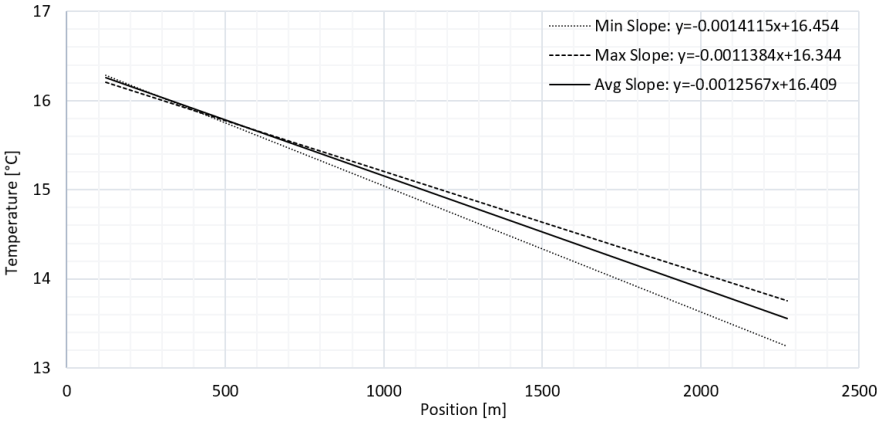

(b)

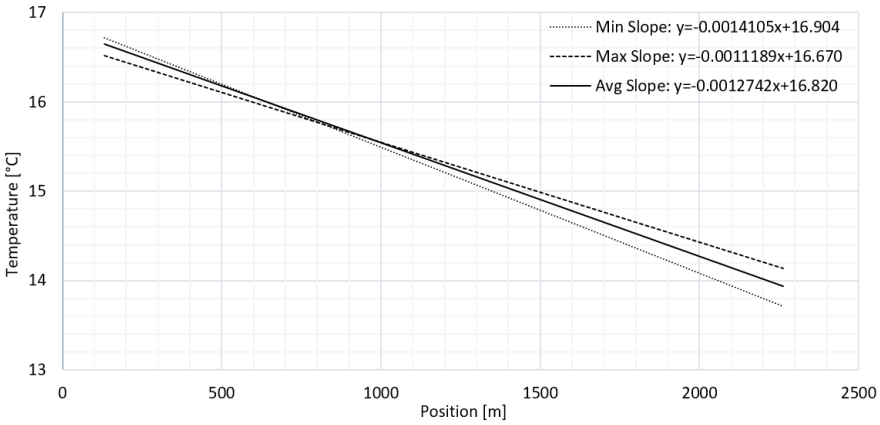

(c)

Figure 3-19. Slope curve of point-wise calibration method in-well at (a) 10 m, (b) 20 m, (c) 30m.

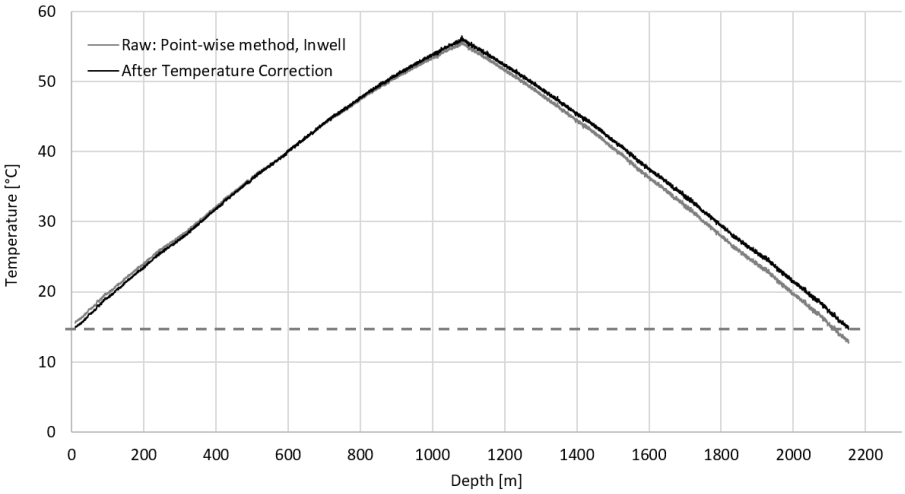

Figure 3-20. Heat profile after point-wise 10 m in-well temperature correction.

3.3.5 Discussion

The summary of the three calibration method is shown in Figure 3-21. As discussed above, the long point calibration method with water tub gave the best slope range and result. Although the point-wise calibration method using the diver had larger slope range compared to long point calibration method, the point-wise calibration method gave reasonable result. When using point-wise method, it is crucial to obtain accurate absolute temperature value where temperature is less likely to fluctuate such as inside the borehole.

The stability curve of all three calibration method is displayed in Figure 3-22. The slope stability curve of long point calibration method has a range of +0.06 degrees and -0.03 degrees. The slope stability curve of point-wise calibration method with in-well of 10 m has a range of +0.35 degrees and -0.25 degrees. The slope stability curve of point-wise calibration method with heat coil has a range of +0.7 degrees and -0.6 degrees. The stability range increases as the depth increase in all three calibration methods, which is expected due to attenuation rate of pulse.

The appropriate temperature error range is within 0.3 degrees, and both water tub and in-well data comes within the range. However, the error range with water tub slope correction is within 0.3 with stability of 0.05 degrees and the temperature error range with diver slope correction is within 0.1 degrees with a stability of 0.3 degrees. Therefore, even though the long point calibration works best, point-wise calibration method can be a useful alternative where long point calibration cannot be done.

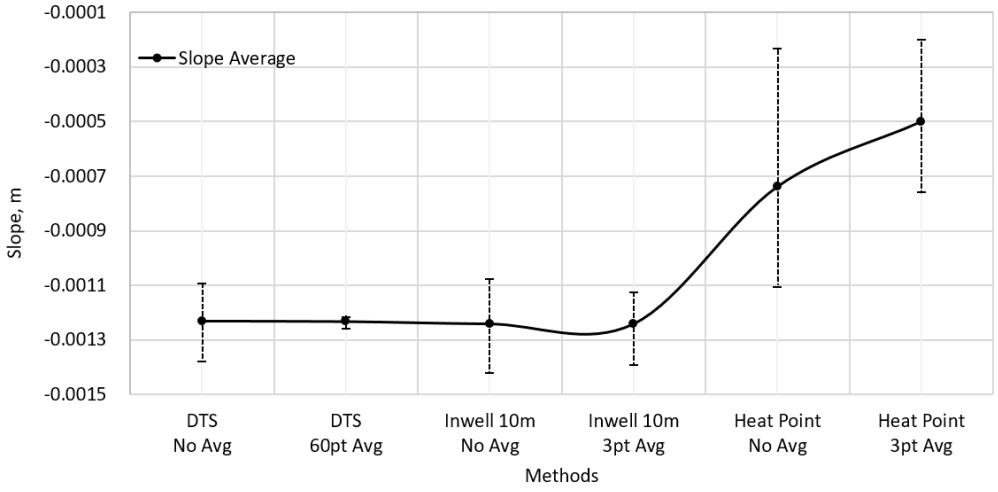

(a)

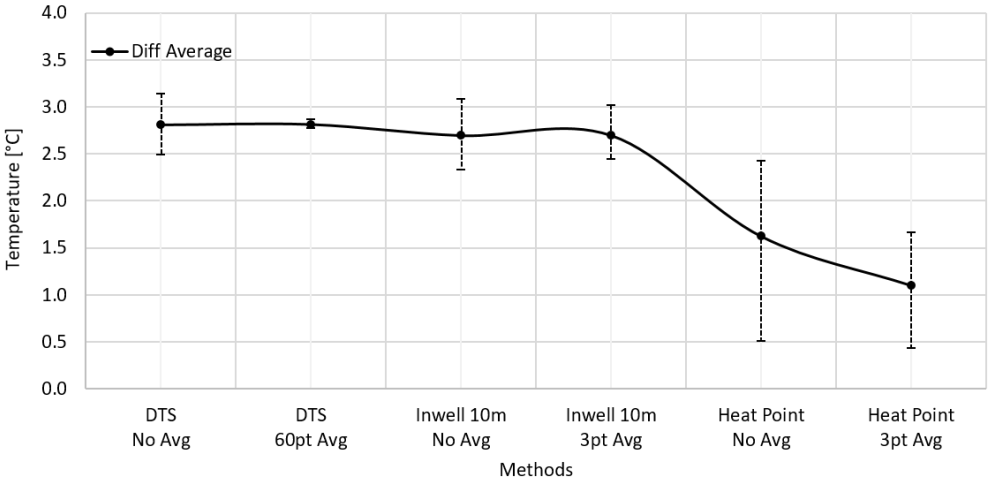

(b)

Figure 3-21. Summary of post-calibration method (a) slope curve and (b) temperature difference curve.

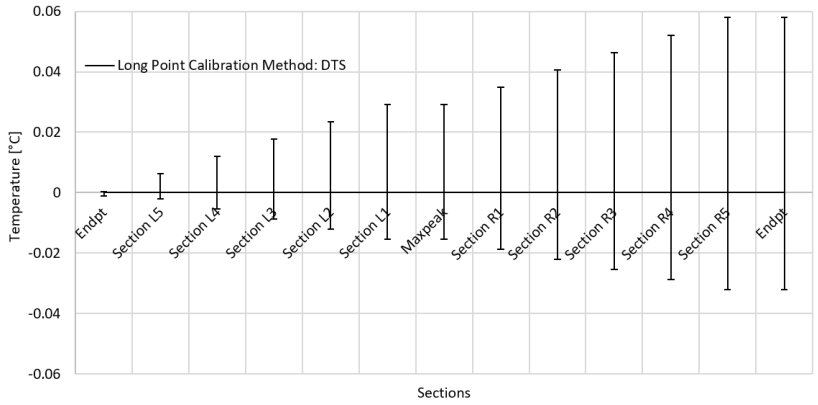

(a)

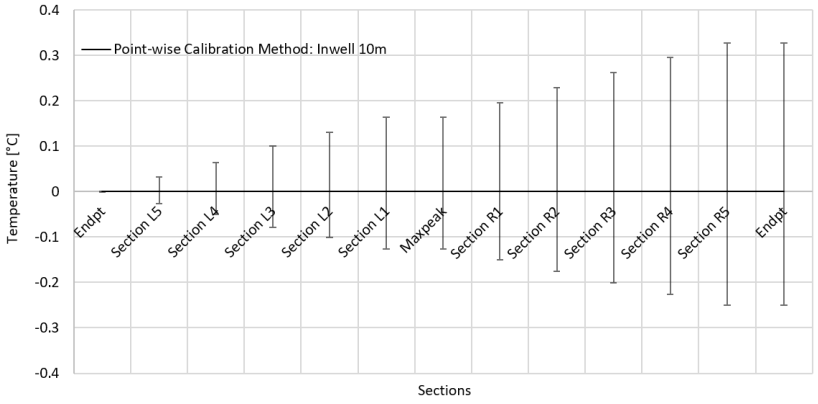

(b)

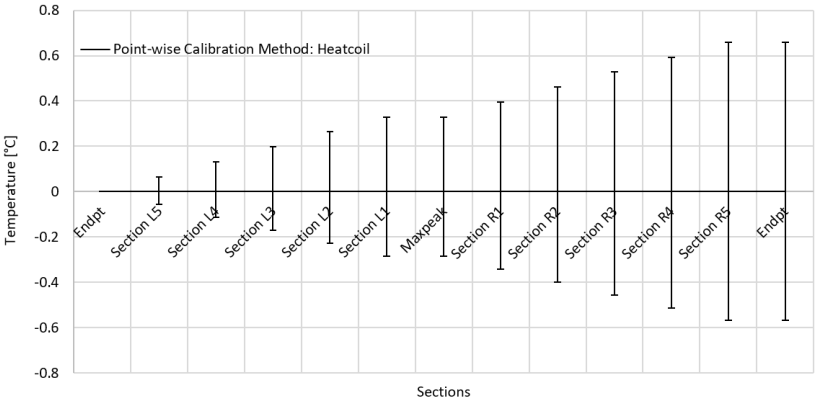

(c)

Figure 3-22. Slope stability of (a) long point calibration with water tub (b) point-wise calibration with in-well and (c) point-wise calibration with heat coil.

Chapter 4. Interpretation of Data

The effects of the gravel pack, injection of fluid, gas lift and curing process are observed. The classic example of a liquid entry is shown in the previous theory section. In Janggi monitoring well, the interpretation of the fiber optic DTS data was necessary for understanding and monitoring the events during well completion. The gravel packing and cementing process are the final critical steps in-well completion that ensure well stability, maintaining well productivity, and proper support of the final casing string. All the fiber optic DTS data were obtained through real-time monitoring during the well completion to monitor the process from JG-M well including, gravel packing, cement injection, chemical reaction, cement curing process, and gas lift process.

The uniqueness of Janggi field data is the continuous real-time monitoring of the whole well completion process from gravel packing to well after completion without well intervention. By utilizing the distributed sensing advantage over point sensor to continuously collect temperature data of the well, continuous heat map of well completion aided in understanding and evaluate the well completion process. The heat map of the data obtained from May 11th to June 4th is shown in Figure 4-1. The anomalies in the data all corresponds to each stage during well completion. The first, second, third and fourth anomaly corresponds to gravel packing, cement injection, gas lift, and cementing operation respectively and each stage shows distinguished anomaly pattern. The anomaly pattern of each process are discussed in detail in the following sections.

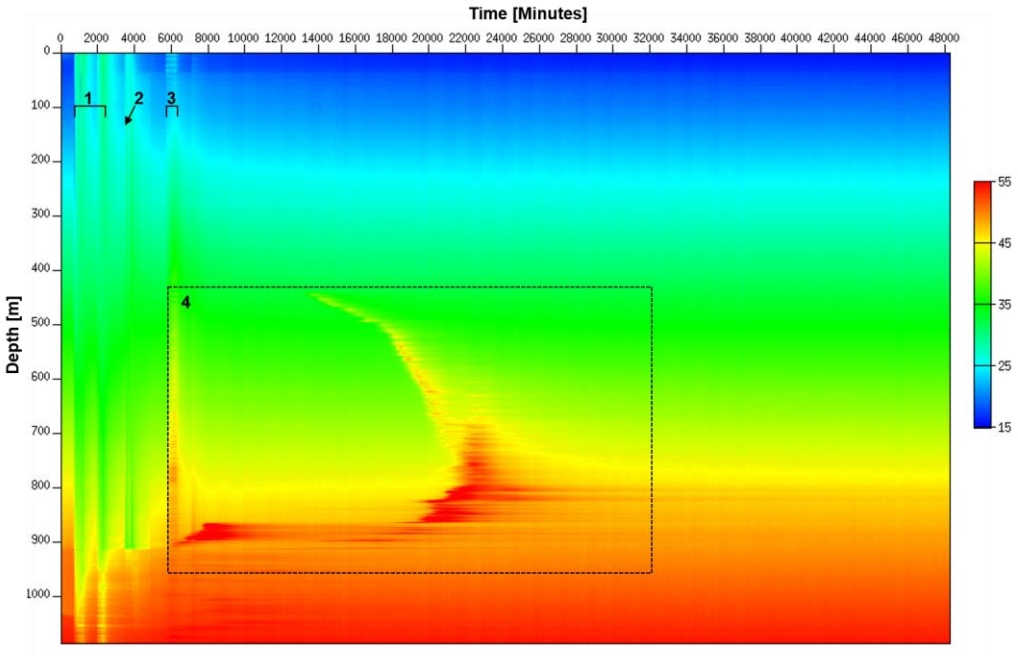

Figure 4-1. Heat map during well completion where the gravel packing is denoted by 1, the cement injection by 2, the gas lift operation by 3 and the cement curing process by 4.

4.1 Gravel packing

There have been monitoring of production in gravel packed completions but monitoring the gravel packing process itself was not yet done (Brown, 2007). Another approach to using DTS besides the conventional gas lift and injection is monitoring of the gravel packing process. The gravel packing process ensures stabilization of the well while minimizing impairment to well productivity. At Janggi Field site, fiber optic cable was connected directly after casing installation to DTS unit, which allowed real-time monitoring of the gravel packing process throughout the entire length of the well. The detailed temperature profile during gravel packing effect can be seen in Figure 4-2 which outlines the major events during the gravel packing process.

The reference data is the temperature profile of end of well completion. The gravel packing process can be delineated by the cooling temperature effect inside the well. Therefore, decreasing of temperature profile compared to reference data is seen. The temperature during the gravel packing process is decreased due to sand being injected directly into the annulus with colder fluids than the fluid inside the well. In the deeper parts of the well, high temperature anomaly with oscillating pattern can be seen due to water circulating but leaving sand to be accumulated and therefore heat transfer is faster because of the sand acting as the connectivity between sand and formation. Therefore, the gravel pack acting as the thermal bridge to the formation. The sand being deposited can be seen by the thermal anomaly traveling up the well. The section where sand is not accumulated does not have this connectivity with formation and cable and still show low temperature trend. The point where the temperature clearly drops marks the top level of the gravel pack. During gravel packing, DTS system was used to monitor the level of the gravel pack to closely match the level of our planned depth of 910 m. A meter spacing

between the stage cement tool and the gravel packed zone was given for safety precaution during the cementing process.

In the low temperature anomaly, the small peaks seem like noise but are due to clamping spaced approximately every 9 m. There are also two notable features due to clamping with high temperature peak anomalies above the top of the gravel packed and lower temperature peak anomalies in the packing zone.

In the case of the high temperature anomalies, inside the casing is warmer than the annulus because the sand was directly injected into the annulus. Consequently, the clamped point of the DTS cable is directly connected to the warmer environment while the other parts are not. In the case of low temperature anomalies, inside the casing is cooler in the packed region. Thus, the clamping point has the reverse effect compared to the previous case. With gravel packing process data, the sensitivity of the DTS data was displayed as it can detect even the smallest changes in the well.

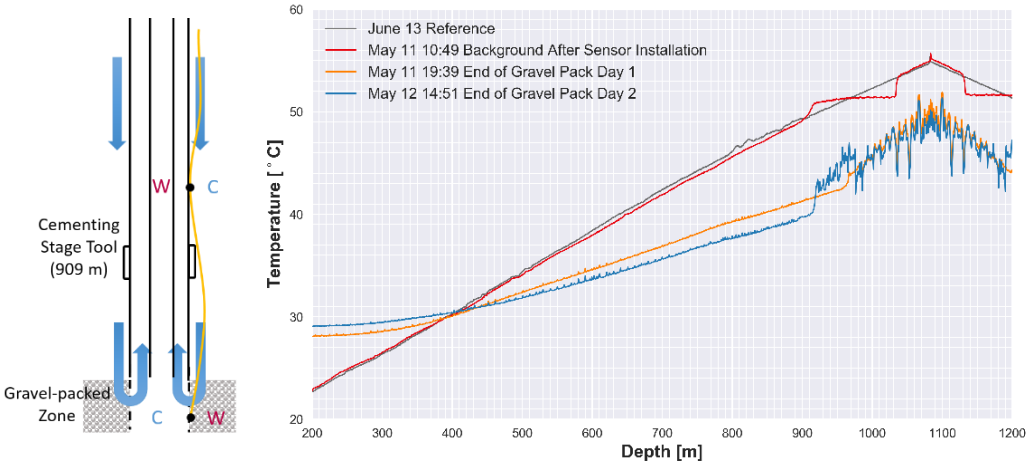

Figure 4-2. Interpretation and temperature profile during the gravel packing operation.

In order to see the global trend during the whole gravel packing process, the heat map of the gravel packing period was drawn. The temperature increase above the gravel-packed zone (top) and the decrease in the gravel packed zone during the operation can be immediately identified. The short burst of cooling at the top may be explained due to either flow change or colder fluid injection or breaks during gravel packing operation. The temperature decrease above the packed zone and increase in the packed zone mark the end of the operation. The similar patterns in two areas mark the gravel packing process and confirm the period of gravel packing, which was carried out over the two days.

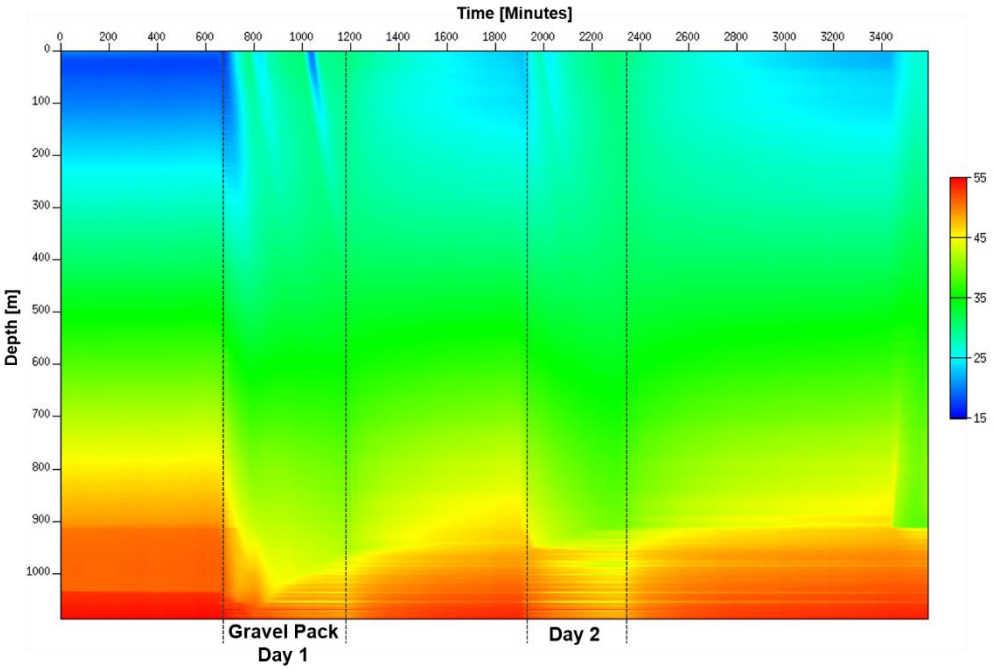

Figure 4-3. Heat map of the gravel packing process.

By monitoring the gravel packing process in real-time, the progression of sand volume can be continually monitored and therefore controlling the amount of sand volume to reach the top of the intended depth. The progression of sand also offers the ability to check for possible plugging as the sand is poured. All these factors optimize the gravel packing process at a field level as the change in temperature is displayed without interrupting the process. The gravel packing process also showed potential for detecting sand production, which is an unwanted event as the accumulation of sand may be detected as a temperature anomaly. The response to sand production can be optimized and diminish the risk of reduced well productivity. In conclusion with real-time monitoring using DTS, the gravel packing process can also be monitored besides the conventional monitoring of injection and gas lift.

4.2 Cement injection and curing process

After the gravel packing operation, the cement slurry was injected to cement the casing in place to complete the well. The cement slurry is a mixture of additives and retarders and carefully mixed by interrogating the purpose of the well. The retarder is used to ensure safe cement placement as it slows down cement settling time. As the temperature increases with depth, the deeper part of the well can cause cements to set prematurely, because higher the temperature, the faster the cement settles down (Sweatman, 2015). Monitoring of injection cement slurry settling down delineate the duration of curing and time of complete curing to move on to the next stage.

The temperature profile of the cement injection process is displayed in Figure 4-4. The temperature before cement injection has a lower temperature than the reference point, which indicates the effect from gravel packing operation still remain and needs more time to recover to the geothermal gradient. As the slurry is injected, the temperature is being gradually lowered until the end of the injection. The end of the cement injection temperature profile may delineate the top of gravel pack as the temperature profile is right after injection. The rate of injection of the slurry is much larger than permeate of slurry passing through the gravel pack. Thus the bottom of the slurry will display later in the temperature profile as the temperature will change more slowly. As the volume of the injection increases, the anomaly widens towards the surface and the temperature slowly recovering after the injection is complete can also be seen in the temperature profile.

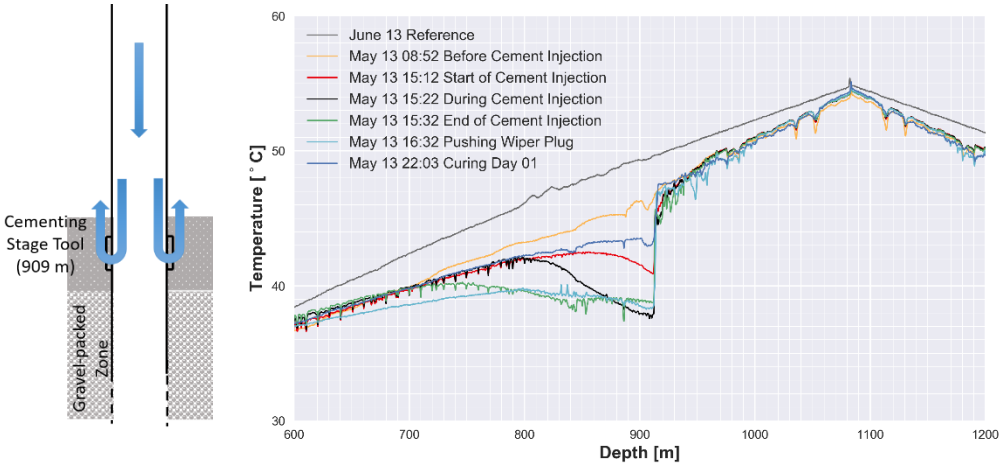

Figure 4-4. Temperature profile of the cement injection and curing.

The curing process took about a month to stabilize due to usage of too much retarder. The major events of curing process from right after injection to a month after injection is shown in Figure 4-5. The red line is right after the installation of the sensors, yellow line before cement operation and black line is after the cement operation, green line is during cement curing and gray line is the complete curing.

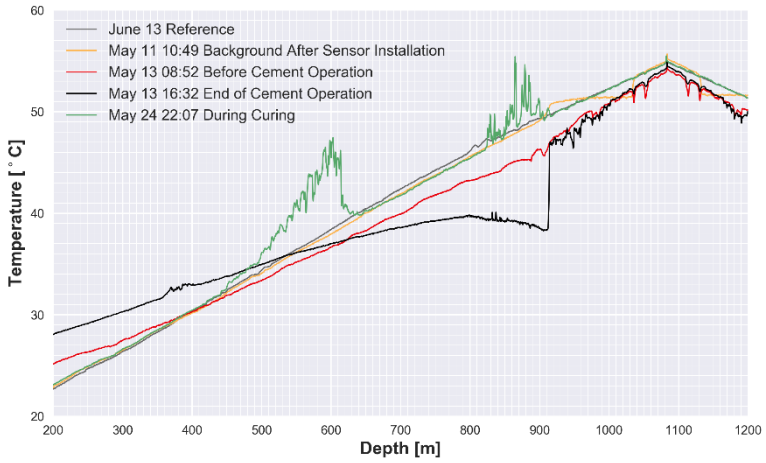

Figure 4-5. Temperature profiles during the curing process of cement.

The green line indicates high temperature anomaly that continues for some period before finally settling down to the background level. The high temperature anomaly is associated with the curing effect and the major events associated with the high temperature anomaly is displayed in Figure 4-6.

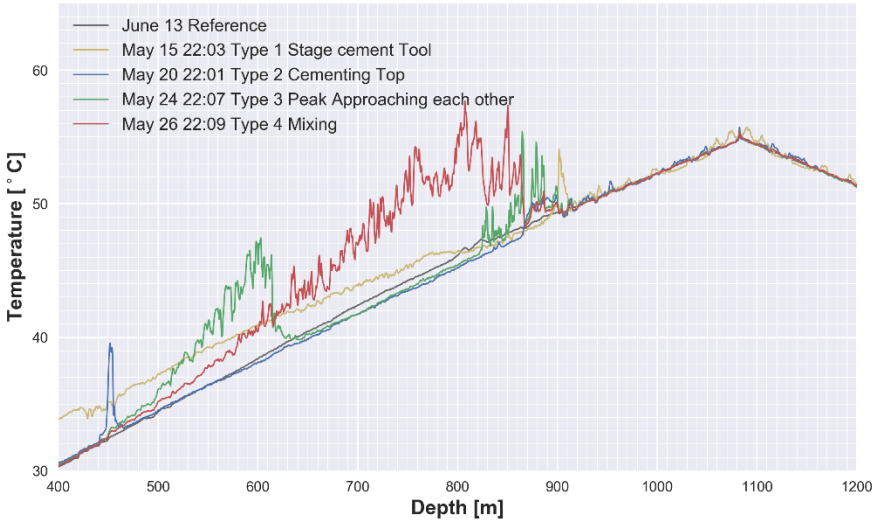

Figure 4-6. Temperature profiles during the curing process in detail.

The yellow line denoted as type 1 is right after the gas lift operation, which explains the remains of the higher temperature anomaly compared to the other types. However, the interesting characteristics are the peak near the stage cement tool which can be interpreted as the start of the curing due to the exothermic process. The effect of the gas lift anomaly is gone in type 2 blue line; however, another peak appears near 450 m. The peak indicates the start of curing from the top. The type 3 green line displays two peaks from the top and bottom boundary. These boundaries move toward each other, indicating the curing from the boundary to the intermediate. The type 4 red line displays the two peaks finally meeting and starting to settle down.

The heat map from Figure 4-1 displays the major trends of the whole cementing operation. The cementing injection interval marked as number two in Figure 4-1. Also, the curing process starting from the stage tool where the increase in temperature migrate from 909 m and upwards. The exact time when the curing started from the 450 m and the time it took from both top and bottom boundary to meet in the intermediate to finally cure can be found with the heat map. Lastly, the time it took to complete cure can be confirmed. The unusual long curing period can be explained by using too much retarder in the slurry.

The cementing is the final critical steps to ensure the stability of the well and monitoring the process in real-time from cement slurry injection to curing optimizes the process. The cement injection data displayed the progression of injection which outlined the rate of injection and injected volume of cement. The progression of cement slurry also offers the ability to check for possible plugging as the cement slurry is injected. After cement injection, the stages of exothermic reaction gave better insight to the curing process. If it had not been for constant monitoring of the entire well, it would have been difficult correlating the unusual anomaly to exothermic reaction due to the settling of the cement. By monitoring the curing process, the time of complete curing could be accurately known by the homogeneity in temperature and allow moving on to the next stage with confidence. Moving onto the next stage before complete curing is not ideal and if further analysis were done before complete curing, interpreting data could become difficult. In conclusion, monitoring the complete curing process throughout the entire length of the well allowed a better understanding of the curing process by analyzing the temperature response to cement.

4.3 Gas lift

The gas lift operation artificially lifts the fluids inside the tubing by injecting high pressure gas, which adds bubbles of compressed air. The gas lift is carried out until the fluids begin to flow to maximized production. In gas lift process, it is difficult to identify which gas lift valve is injecting and its injection points thus able to optimize gas lift operation at a field level. However, monitoring the gas lift process with DTS solves the challenges gas lift process is facing. Conventionally, DTS is used as a surveillance tool to monitor the gas lift process and is identified with the oscillating pattern. The gas injection points and depth can also be delineated from the gas lift data (Hemink & van der Horst, 2018).

In Janggi, the gas lift process was carried out after cement injection but during cement curing. During the gas lift, the N_2 gas was released, and the fluid was pulled upwards due to pressure. The major events of one cycle of gas lift operation is displayed in Figure 4-7. The temperature increased during gas lift operation in the data below 791.90 m. The increase in temperature is due to the deeper and warmer reservoir being pulled up. The high temperature associated with gas lift operation has a highly oscillating pattern. In our data, the conventional oscillating pattern was observed but had different amplitude range between above and below 791.90 m. The difference in amplitude of the oscillation is due to heat conductivity of the different casing material. The 791.90 m is the transition point of different casing material from steel casing to FRP casing. Considering that steel casing has higher heat conductivity than FRP casing, higher amplitude oscillation is observed.

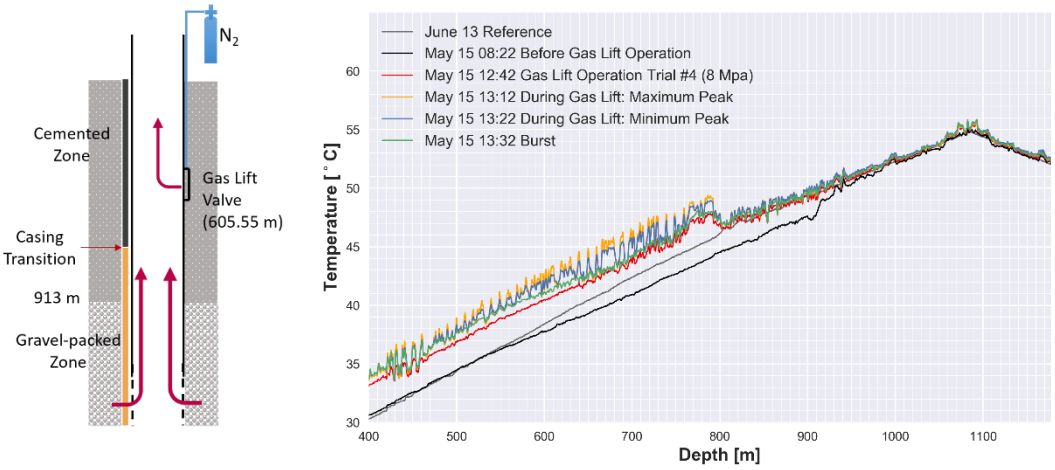

Figure 4-7. Temperature profile of the gas lift in May.

The heat map during the gas lift cycles is displayed in Figure 4-8 to grasp the global trend during the gas lift. The area inside the two dashed line is the period during gas lift operation. The number of repeated patterns during gas lift matches the number of gas lift cycles was done, which was eight cycles. The width of each repeated patterns is the duration of each cycle. Even after the gas lift operation was finished, its effect lasted a day to return to temperature before the gas lift operation began. The temperature did not completely recover due to the starting of curing process near 900m during the middle of gas lift operation.

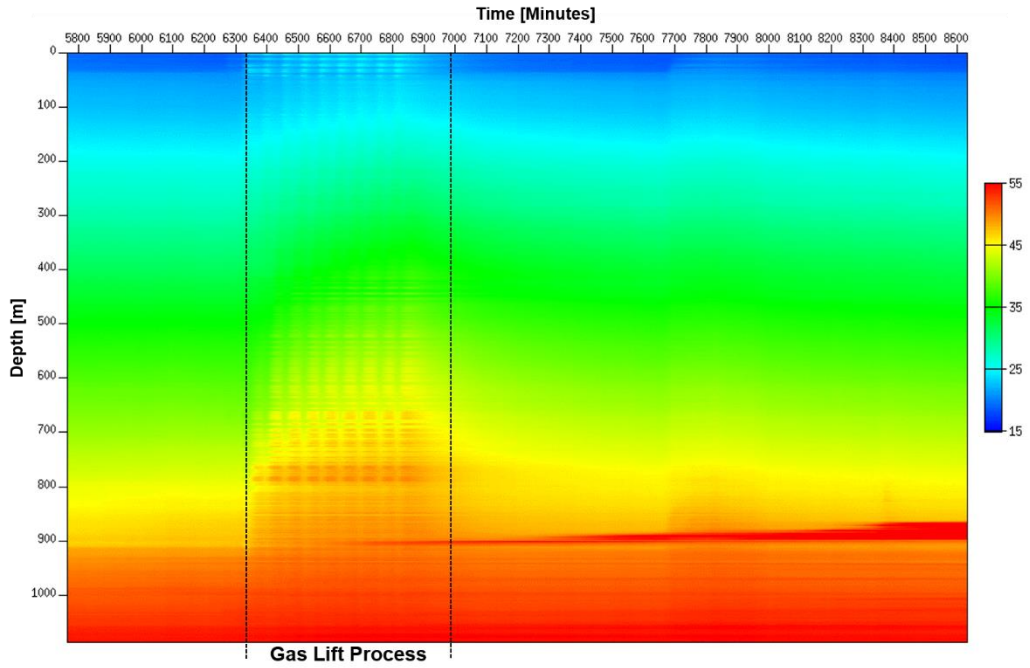

Figure 4-8. Heat map of entire gas lift operation from May and shows effects lasting well after the operation.

In our gas lift data, the conventional oscillation patterns were observed with clamped points displaying better thermal coupling to production tubing. However, in our gas lift data, absolute depth point could be delineated due to using two difference casing material. The absolute depth point supported depth calibration in reducing uncertainty in depth calibration. Since complete gas lift process was collected, the number of gas lift and duration of each cycle could be determined as well. The DTS data has the potential to detect multiple points of injection and determine gas rate through each injection point. All these are possible as the event is happening and require no shut-in when measuring DTS temperature data. Therefore, DTS helps capture the temperature response thus the entire length of the well simultaneously as the event is happening.

Chapter 5. Conclusion

In this thesis, post-calibration methods in terms of depth calibration and temperature calibration of the distributed temperature system were discussed to interpret entire well completion process with DTS data. The objective was to overcome unavoidable depth mismatch between DTS and true depth. The second objective of calibration was to present more practical calibration method in the field. The third objective was to demonstrate the applicability of DTS as a powerful tool in monitoring the well completion process and optimization of each process.

After installation of the fiber optic cable, matching the cable location to DTS is difficult without perturbation from an external source such as water or heat. The depth uncertainty is an avoidable problem on the field. Therefore, in this paper, the uncertainty in depth calibration was reduced by confirming with gas lift data, which delineated the known absolute casing material transition depth. Two methods for depth correction were explored from statistically distributing and ratio statistically distribution method. In our case, there was only a small difference between the two methods. By redistribution of the sampling interval by using known position, in our case, the transition from FRP to steel casing at 791.90 m, the difference to true depth was only 0.036 m. Our expected depth of the top of the gravel pack 911 m was at 913.259 m, and top of cement injection near 910 m was at 912.003 m. During installation, 1 m difference between the top of cement and top of gravel pack was also seen in DTS data after the depth correction.

For temperature calibration, more practical calibration method after installation is compared to conventional calibration before installation. Three different post-calibration methods were explored including long point calibration method to point-

wise calibration method. It is best to calibrate before installation due to uncertainty during development. However, post temperature calibration after installation is within an acceptable range of error. In post-calibration, obtaining accurate absolute value is an important factor. Therefore, in order to find an accurate absolute value, various experiments were done to find the absolute value with long point and pointwise experiments. It was concluded that the long point, water tub experiment displayed the most preferable result with error range within 0.3 degrees with stability of 0.05 degrees. However, point-wise method with in-well is another valid option where error range with within 0.3 degrees with stability of 0.3 degrees where long point method cannot be done.

Monitoring the gravel packing process can be added as another application usage of DTS. The sand progression up the well was displayed which can delineate possible plugging as sand is poured. The potential for detecting accumulation was displayed as top to the gravel pack could be identified by clear temperature drop. In cementing, the injected volume with migration of low temperature anomaly was monitored which optimized the process by outlining rate of injection and injected volume. It can also monitor for possible plugging during injection. The curing process was identified by the high temperature anomaly exothermic reaction. In our case, the curing started from the top and bottom boundary and proceeding to the intermediate zone. Monitoring the complete curing process allowed insight to how curing was carried out. The conventional highly oscillating patterns associated to gas lift process was displayed in our data as well. Monitoring the gas lift process helped in not only identifying which gas lift valve is injecting but aid in reducing depth uncertainty by delineating casing transition point. In conclusion, monitoring complete well completion without well intervention using DTS displayed to be powerful tool. Therefore, innovative use of DTS system offers potential for optimizing the procedure by monitoring the complete operation in real-time.

References

Bao, X., & Chen, L. (2012). Recent Progress in Distributed Fiber Optic Sensors. Sensors, 12(7), 8601-8639. doi: 10.3390/s120708601

Bense, V., Read, T., Bour, O., Le Borgne, T., Coleman, T., & Krause, S. et al. (2016). Distributed Temperature Sensing as a downhole tool in hydrogeology. Water Resources Research, 52(12), 9259-9273. doi: 10.1002/2016wr018869

Brown, G. A., Kennedy, B., & Meling, T. (2000, January 1). Using Fiber optic Distributed Temperature Measurements to Provide Real-Time Reservoir Surveillance Data on Wytch Farm Field Horizontal Extended-Reach Wells. Society of Petroleum Engineers. doi:10.2118/62952-MS

Brown, G. A., Pinzon, I. D., Davies, J. E., & Mammadkhan, F. (2007, January 1). Monitoring Production from Gravel-Packed Sand-Screen Completions on BP's Azeri Field Wells Using Permanently Installed Distributed Temperature Sensors. Society of Petroleum Engineers. doi:10.2118/110064-MS

Brown, G., Carvalho, V., Wray, A., Smith, D., Toombs, M., & Pennell, S. (2004, January 1). Monitoring Alternating CO2 and Water Injection and Its Effect on Production in a Carbonate Reservoir Using Permanent Fiber optic Distributed Temperature Systems. Society of Petroleum Engineers. doi:10.2118/90248-MS

Clanton, R. W., Haney, J. A., Pruett, R., Wahl, C. L., Goiffon, J. J., & Gualtieri, D. (2006, January 1). Real-Time Monitoring of Acid Stimulation Utilizing a Fiber optic DTS System. Society of Petroleum Engineers. doi:10.2118/100617-MS

Coleman, T., Parker, B., Maldaner, C., & Mondanos, M. (2015). Groundwater flow characterization in a fractured bedrock aquifer using active DTS tests in sealed boreholes. Journal Of Hydrology, 528, 449-462. doi: 10.1016/j.jhydrol.2015.06.061

Crisp, J., & Elliott, B. (2005). Introduction to Fiber optics. Amsterdam: Newnes.

Fang, Z., Chin, K., Qu, R., & Cai, H. (2012). Fundamentals of Optical Fiber Sensors (1st ed.). New Jersey: Wiley.

Fryer, V. I., Dong, S., Otsubo, Y., Brown, G. A., & Guilfoyle, P. (2005, January 1). Monitoring of Real-Time Temperature Profiles Across Multizone Reservoirs during Production and Shut in Periods Using Permanent Fiber optic Distributed Temperature Systems. Society of Petroleum Engineers. doi:10.2118/92962-MS

Hartog, A. (1983). A distributed temperature sensor based on liquid-core optical Fibers. Journal Of Lightwave Technology, 1(3), 498-509. doi: 10.1109/jlt.1983.1072146

Hartog, A. (2017). An introduction to distributed optical fiber sensors. Boca Raton: CRC Press, Taylor & Francis Group.

Hausner, M., Suárez, F., Glander, K., Giesen, N., Selker, J., & Tyler, S. (2011). Calibrating Single-Ended Fiber optic Raman Spectra Distributed Temperature Sensing Data. Sensors, 11(11), 10859-10879. doi: 10.3390/s111110859

Hemink, G., & van der Horst, J. (2018). On the Use of Distributed Temperature Sensing and Distributed Acoustic Sensing for the Application of Gas Lift Surveillance. SPE Production & Operations. doi: 10.2118/191130-pa

Hurtig, E., Groβwig, S., & Kühn, K. (1996). Fiber optic temperature sensing: application for subsurface and ground temperature measurements. Tectonophysics, 257(1), 101-109. doi: 10.1016/0040-1951(95)00124-7

Kim, K., Oh, J., Han, W., Park, K., Shinn, Y., & Park, E. (2018). Two-phase flow visualization under reservoir conditions for highly heterogeneous conglomerate rock: A core-scale study for geologic carbon storage. Scientific Reports, 8(1). doi: 10.1038/s41598-018-23224-6

Schlumberger. (2009). The Essentials of Fiber optic Distributed temperature Analysis (pp. 1- 63). Sugar land: Schlumberger Educational services.

Silixa. (2016). XT-DTS Hardware Manual 1.3. UK: Silixa.

Smolen, J., & van der Spek, A. (2003). Distributed Temperature Sensing - A DTS Primer for Oil & Gas Production (1st ed., pp. 1-50). Missouri City: Shell.

Sweatman, R. (2015). Well Cementing Operations. Houston: IADC.

Tyler, S., Selker, J., Hausner, M., Hatch, C., Torgersen, T., Thodal, C., & Schladow, S. (2009). Environmental temperature sensing using Raman spectra DTS Fiber optic methods. Water Resources Research, 45(4). doi: 10.1029/2008wr007052

Wang, H. (2013). A fiber optic system for distributed temperature sensing based on raman scattering (Masters of philosophy). University of Bradford.

Wang, Y. (2012). A Quasi-distributed Sensing Network Based on Wavelength-Scanning Time-division Multiplexed Fiber Bragg Gratings (Ph.D). Virginia Polytechnic Institute.

Weaver, M. A., Kragas, T. K., Burman, J., Copeland, D. L., Phillips, B., & Seagraves, R. (2005, January 1). Installation and Application of Permanent Downhole Optical Pressure/Temperature Gauges and Distributed Temperature Sensing in Producing Deepwater Wells at Marco Polo. Society of Petroleum Engineers. doi:10.2118/95798-MS

초 록

시추공 완결과정이 가지는 특징적인 온도변화 양상을 고찰하고, 시추공 완결과정을 모니터링 방법론으로서의 DTS의 적용성을 확인하기 위해 장기분지에 국내 최초로 구축된 지중저장 CO_2 관측정의 완결 과정에서 얻어진 DTS 자료를 분석하였다. 광섬유 내를 전파하는 빛의 산란에 온도가 미치는 영향에 기반하는 DTS 자료는 반드시 실제 온도를 이용하여 교정되어야 할 뿐만 아니라, 광섬유센서 케이블 설치 과정에서 불가피하게 발생하는 깊이오차도 보정되어야 하기 때문에, 이 연구에서는 깊이 오차와 여러 온도의 설치 후 교정 방법들도 비교 분석하였다.

광섬유 센서 케이블을 설치할 때, 케이블의 꼬임에 의해 불가피 하게 발생하는 깊이 오차는 시추공의 총길이 (TD; Total Depth) 대비 광케이블 길이오차의 비율에 따라 온도 측정점 심도를 보상하는 전통적인 방식을 취하였고, 이를 철제 케이싱과 FRP 케이싱 연결부 깊이와 같은 사전정보와 gas lift 자료에서 케이싱 연결구간에서 나타나는 특징적인 온도변화 형태와 비교함으로써 보정 방식의 효율성을 확인하였다.

효과적인 온도의 후교정을 제시하기 위해서는 기존의 구간 기반(long-point) 전교정 방법과 더불어 점 기반(point-wise) 후교정 방법을 비교 분석하였다. 사용된 펄스폭에 의해 정의되는 분해능셀(resolution cell)이나 게이지 길이(gauge length)보다 긴 일정 구간을 물에 담그는 방식의 전교정 방식은 예상대로 가장 좋은 결과를 보여주었다. 그러나 점 기반 후교정 방식도 구간 기반 방식에 준하는 결과를 보여줌으로써, 구간 기반 방식의

사전 또는 사후 교정이 어려운 경우 이를 대체할 수 있는 효과적인 방법이 될 수 있음을 확인할 수 있었다.

DTS로 실시간 측정된 온도 프로파일은 관측정 완결을 위한 각 과정들이 각각 특징적인 온도 변화(anomaly)로 나타남을 보여준다. 자갈패킹의 경우, 패킹구간에서 높은 온도 변화로 확인되며, 이러한 변화를 통해 패킹된 모래층의 높이 모니터링이 가능하다. 시멘팅 과정의 경우, 주입된 시멘트의 상대적으로 낮은 온도 변화로 확인되며, 온도변화 전파 양상을 통해 주입된 시멘트의 부피 모니터링이 가능하다. 시멘트의 경화는 경화 과정에서의 발열 반응이 관찰되었으며, 시간에 따른 온도변화를 통해 경화의 진행을 확인하였다. Gas-lifting 과정은 매우 심한 진동을 동반한 고온 변화로 확인할 수 있었다. 이를 종합할 때, DTS를 이용한 실시간 온도 프로파일 측정은 시추공 완결 과정 중 공정의 진행상황 모니터링 뿐만 아니라 이를 활용한 공정의 제어 및 최적화를 위한 효과적인 방법이 될 수 있을 것으로 기대된다.

주요어 : 분산형 온도 측정, DTS, 분산형 측정, 온도 보정, 깊이 보정, 광섬유 센서, 완결 공정, 장기 현장

학 번 : 2016-21301